Interior penalty discontinuous Galerkin method for coupled elasto-acoustic media

Yohann Dudouit, Luc Giraud, Florence Millot, Sébastien Pernet

Interior penalty discontinuous Galerkin method for coupled elasto-acoustic media

Yohann Dudouit, Luc Giraud, Florence Millot, Sébastien Pernet

RESEARCH REPORT
N° 8986
December 2016
Project-Teams HiePACS

ISSN 0249-6399 ISRN INRIA/RR--8986--FR+ENG

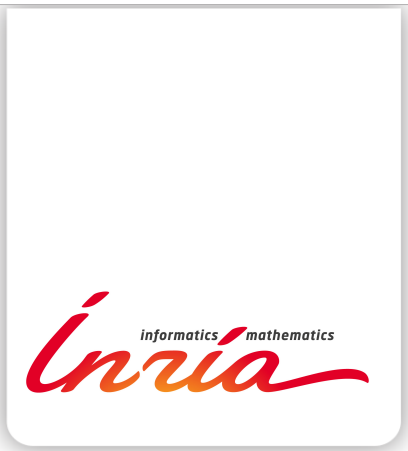

Interior penalty discontinuous Galerkin method for coupled elasto-acoustic media

Yohann Dudouit*, Luc Giraud†, Florence Millot‡,

Sébastien Pernet§

Project-Teams HiePACS

Research Report n° 8986 — December 2016 — 29 pages

Abstract: We introduce a high order interior penalty discontinuous Galerkin scheme for the numerical solution of wave propagation in coupled elasto-acoustic media. A displacement formulation is used, which allows for the solution of the acoustic and elastic wave equations within the same framework. Weakly imposing the correct transmission condition is achieved by the derivation of adapted numerical fluxes. This generalization does not weaken the discontinuous Galerkin method, thus *hp*-non-conforming meshes are supported. Interior penalty discontinuous Galerkin methods were originally developed for scalar equations. Therefore, we propose an optimized formulation for vectorial equations more suited than the straightforward standard transposition. We prove consistency and stability of the proposed schemes. To study the numerical accuracy and convergence, we achieve a classic plane wave analysis. Finally, we show the relevance of our method on numerical experiments.

Key-words: discontinuous Galerkin, interior penalty, elasto-acoustic

* CERFACS-Inria lab. on High Performance Computing, France
† Inria, France
‡ CERFACS, France
§ The french aerospace lab, ONERA, France

RESEARCH CENTRE
BORDEAUX – SUD-OUEST

200 avenue de la Vielle Tour
33405 Talence Cedex

Schéma Galerkin Discontinu avec pénalisation intérieure pour des milieux couplés élastique-acoustique

Résumé : Nous introduisons un shéma de type Galerkin discontinu d'ordre élevé avec pénalisation intérieure pour la simulation d'ondes se propagant dans des mileux couplés elastique-acoustique. Une formuation en déplacement est utilisée, qui permet de traiter dans un même cadre les équations acoustiques et élastiques. La condition de transmission entre les deux mileux est imposée de façon faible en dérivant un terme de flux adapté. Cette généralisation n'affaiblit pas l'approche Galerkin discontinue; en particulier, la formulation supporte des maillages *hp* non conformes. Les méthodes de Galerkin discontinu avec pénalisation intérieure ont été originellement développées pour des équations scalaires. Nous proposons dans ce travail une formulation optimisée pour des équations vectorielles mieux adaptées qu'une re-écriture immédiate du cas scalaire en vectoriel. Nous montrons que le schéma proposé est stable et consistant et étudions sa précision et sa convergence via une analyse classique par ondes planes. Enfin, nous illustrons la pertinence de notre méthode au travers de quelques exemples numériques de cas tests synthétiques élastique-acoustique couplés.

Mots-clés : Galerkin discontinu, pénalisation intérieure, elasto-acoustique

1 Introduction

We introduce a discontinuous Galerkin method optimized for wave propagation in elasto-acoustic media. The formulation of this method was first motivated by the simulation of hydro-fractures in geophysics. Nonetheless, our approach to elasto-acoustic media could be applied to other fields, *e.g.*, ultra-sounds waves in biological tissues [1], or vibrations of solid structures immersed in surrounding fluids [4]. The standard approach to model hydro-fractures is to use equivalent models. However, these equivalent models are based on asymptotic models and hide some phenomena, *e.g*, wave scattering. Thus, a rigorous modeling is mandatory. Our approach is relevant for media with a large number of small scale elasto-acoustic areas. For large elasto-acoustic coupling, *e.g.*, earth ocean, different approaches would be better suited.

Geophysics requires accurate, efficient and scalable parallel numerical methods. The accuracy challenge comes from the high distance (in terms of wavelength) waves have to travel. In order to control dispersion and dissipation errors, high order methods need to be used. Due to the large number of degrees of freedom the methods have to be computationally efficient. Computational efficiency also requires scalable parallelization. However, coupling different methods result in a much more challenging scalable parallelization. Therefore, this challenge has led us to consider methods that handle elasto-acoustic media in an unified framework. When one wants to model small details of the media, such as hydro-fractures *hp*-non-conforming meshes become a highly desirable feature. Most numerical methods can deal with some of the previous challenges, however few methods can comply with all the constraints associated with all these challenges.

A large number of numerical methods for acoustic and elastic wave propagation exists. Even though finite differences [28, 24, 18] are widely used in the geophysics community, each of the above challenges is an active area of research, especially dealing with elasto-acoustic interfaces [17] and with *hp*-non-conforming meshes. The finite volume methods [12, 13, 16] suffer from their lack to support at the same time elasto-acoustic media and high order [11, 25] . The finite element methods [29, 2] and spectral element methods [15, 8, 20] also suffers from a lack of a natural way to deal with elasto-acoustic interfaces. However, there exists methods that deal with elasto-acoustic interfaces [14, 3] but their computational cost lead to a challenging scalable parallelization.

In contrast discontinuous Galerkin methods [21, 10] deal with most of these challenges in a natural manner. Discontinuous Galerkin methods are often discarded due to their relative high computational cost on simple physics media. However, their ability to deal in a natural manner with most of these challenges make them very attractive. The only challenge that does not come naturally with discontinuous Galerkin methods is the ability to handle elasto-acoustic interfaces. In this work, we propose a discontinuous Galerkin method that handles elasto-acoustic interfaces without any additional cost for the second order wave equation. Avoiding the computational heterogeneities coming when coupling methods, we keep the DG methods computation homogeneity unchanging the efficient parallelization of DG methods. Contrary to [27] where the formulation is based on stress-velocity formulation, our approach is based on the displacement formulation, saving a lot of degrees of freedom.

The paper is organized as follows. In Section 2, we introduce our interior penalty discontinuous Galerkin method for elasto-acoustic problems. In Section 3, we propose an optimized formulation of the IPDG for vectorial problems. In Section 4, we show the relevance of our approach for hydro-fractures on numerical results. Finally, we conclude in Section 5.

2 IPDG optimized for hydro-fractures

2.1 Model problem

Let Ω be a polygonal domain of $\mathbb{R}^d$, $d = 1, 2$ or 3 such that $\Omega = \Omega_e \cup \Omega_a$ with $\Omega_e \cap \Omega_a$ and $\partial\Omega_a \cap \partial\Omega = \emptyset$ (see Fig. 1). The domains Ω_e and Ω_a are the elastic and the acoustic media, respectively. The boundary $\partial\Omega$ are grouped into two disjoints sets Γ_D and Γ_N. Moreover, we define the elasto-acoustic interface $\Gamma := \partial\Omega_e \cap \partial\Omega_a$. Finally, we denote by $\mathbf{n}$ the unit outward normal to Ω or Ω_a .

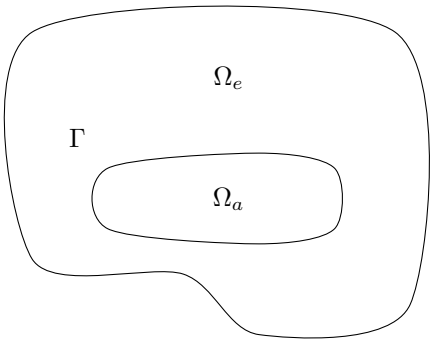

Figure 1: Domain Ω.

We consider the following elasto-acoustic transmission problem:
Find $\mathbf{u} : \Omega \times [0, T] \to \mathbb{R}^d$ such that

$$\begin{cases} \rho\dfrac{\partial^2\mathbf{u}}{\partial t^2} - \mathrm{div}(\sigma(\mathbf{u})) = \mathbf{f}, & \text{in } \Omega, \\ \mathbf{u} = 0, & \text{on } \Gamma_D, \\ \sigma(\mathbf{u}) \cdot \mathbf{n} = 0, & \text{on } \Gamma_N, \\ \mathbf{u}(\mathbf{x}, 0) = \mathbf{u}_0(\mathbf{x}), & \forall \mathbf{x} \in \Omega, \\ \dfrac{\partial\mathbf{u}}{\partial t}(\mathbf{x}, 0) = \mathbf{v}_0(\mathbf{x}), & \forall \mathbf{x} \in \Omega, \end{cases} \tag{2.1}$$

where $\sigma(\cdot)$ is the Cauchy stress tensor associated with the elastic media, $\mathbf{u}(\mathbf{x}, t)$ is the displacement field, ρ is the mass density, $\mathbf{f} \in \mathrm{L}^2(\Omega)$ and $\mathbf{u}_0, \mathbf{v}_0$ are the initial conditions.

In this paper, we consider an isotropic elastic materials, *i.e.*, the Cauchy stress tensor can be written as:

$$\sigma(\mathbf{u}) := 2\mu e(\mathbf{u}) + \lambda tr(e(\mathbf{u}))I, \tag{2.2}$$

where $e(\mathbf{u}) = \frac{1}{2}(\nabla\mathbf{u} + \nabla\mathbf{u}^T)$ is the strain tensor, λ and μ are the Lamé parameters, I the identity matrix and $tr(.)$ the trace function.
We can write (2.1) in an equivalent form such that all the different physics appear:

Find $\mathbf{u} : \Omega \times [0,T] \to \mathbb{R}^d$ such that

$$\begin{cases} \rho\dfrac{\partial^2 \mathbf{u}}{\partial t^2} - \mathrm{div}(\sigma(\mathbf{u})) = \mathbf{f}, & \text{in } \Omega_e, \\ \rho\dfrac{\partial^2 \mathbf{u}}{\partial t^2} - \nabla(\lambda \mathrm{div}\mathbf{u}) = \mathbf{f}, & \text{in } \Omega_a, \\ \mathbf{u}_{|\Omega_e} \cdot \mathbf{n} - \mathbf{u}_{|\Omega_a} \cdot \mathbf{n} = 0, & \text{on } \Gamma, \\ \sigma(\mathbf{u}_{|\Omega_e})\mathbf{n} + \lambda \mathrm{div}(\mathbf{u}_{|\Omega_a}) = 0, & \text{on } \Gamma, \\ \mathbf{u} = 0, & \text{on } \Gamma_D, \\ \sigma(\mathbf{u}) \cdot \mathbf{n} = 0, & \text{on } \Gamma_N, \\ \mathbf{u}(\mathbf{x},0) = \mathbf{u}_0(\mathbf{x}), & \forall \mathbf{x} \in \Omega, \\ \dfrac{\partial \mathbf{u}}{\partial t}(\mathbf{x},0) = \mathbf{v}_0(\mathbf{x}), & \forall \mathbf{x} \in \Omega. \end{cases} \tag{2.3}$$

The main difficulty when one attempts to have an unified method for elasticity and acoustic is that the two equations do not impose the same continuity on the displacement and its derivatives. The classical weak formulation associated with the model (2.3) is defined by:

Find $\mathbf{u} \in \mathbf{V} := \{\mathbf{v} \in \mathbf{L}^2(\Omega) \,:\, \mathbf{v}_{|\Omega_e} \in \mathbf{H}^1(\Omega_e),\, \mathbf{v}_{|\Omega_a} \in \mathbf{H}(\mathrm{div}\,, \Omega_a),\, [\![\mathbf{v} \cdot \mathbf{n}]\!]_\Gamma = 0 \text{ and } \mathbf{v}_{|\Gamma_D} = 0\}$ such that $\forall \mathbf{v} \in \mathbf{V}$,

$$\int_\Omega \rho \frac{\partial^2 \mathbf{u}}{\partial t^2} \cdot \mathbf{v}\, d\mathbf{x} + \int_{\Omega_e} \sigma(\mathbf{u}) \,:\, \nabla \mathbf{v}\, d\mathbf{x} + \int_{\Omega_a} \lambda \mathrm{div}\mathbf{u}\, \mathrm{div}\mathbf{v}\, d\mathbf{x} = \int_\Omega \mathbf{f} \cdot \mathbf{v}\, d\mathbf{x}. \tag{2.4}$$

Setting $\mu = 0$ would impose too much continuities with standard numerical methods, *e.g.*, finite element methods or finite difference methods. Furthermore, even for standard DG methods where all continuities are implicit, continuities which have no place in the case of an elasto-acoustic interface are imposed. However, we will show how a modification of the IPDG method for elastodynamic enable to handle such configurations.

2.2 IPDG for elasto-acoustic problems

In this part, we propose a discontinuous Galerkin approximation which treats in an unified framework the elastodynamic, the acoustic and thus the hydro-fracture problem. First, we recall the standard IPDG approximation of the pure elastic operator and we next explain how to modify it on order to take into account the elasto-acoustic medium.

2.2.1 IPDG for elastic problems

We will introduce now the formal construction of several standard discontinuous Galerkin formulations called interior penalty discontinuous Galerkin. We refer to [21] for a deeper insight into these methods.

Let Ω be subdivided into elements, we denote this partition by $\mathcal{T}_h$. We denote by $\mathcal{F}_h$ the set of all faces. A face shared by two elements is called an interior face, we denote by $\mathcal{F}_h^{\mathcal{I}}$ the set of all interior faces. Likewise, a boundary face of $K \in \mathcal{T}_h$ is $\partial K \cap \partial\Omega$, we denote by $\mathcal{F}_h^{\mathcal{B}}$ the set of all boundary faces. We also denote by $\mathcal{F}_K$ the set of faces of an element K.

For any piecewise smooth function $\mathbf{v}$, we define the following trace operators. Let $F \in \mathcal{F}_h^{\mathcal{I}}$ be an interior face shared by two neighboring elements K_1 and K_2. We assume that the normal vector $\mathbf{n}_F$ to the face F is oriented from K_1 to K_2, we define the average and jump of $\mathbf{v}$ on F by

$$\{\!\{\mathbf{v}\}\!\} := \frac{1}{2}(\mathbf{v}|_{K_1} + \mathbf{v}|_{K_2}), \quad [\![\mathbf{v}]\!] := \mathbf{v}|_{K_1} - \mathbf{v}|_{K_2},$$

respectively.
Let $F \in \mathcal{F}_h^{\mathcal{B}} \cap \Gamma_D$, we define $\{\!\{\mathbf{v}\}\!\} := \mathbf{v}$ and $[\![\mathbf{v}]\!] := \mathbf{v}$.
Let $F \in \mathcal{F}_h^{\mathcal{B}} \cap \Gamma_N$, we define $\{\!\{\sigma(\mathbf{v})\mathbf{n}\}\!\} := 0$ and $[\![\sigma(\mathbf{v})\mathbf{n}]\!] := 0$.

We now explain the formal construction of our DG approximation of the second order operator $-div(\sigma(\mathbf{u}))$. Let $\mathbf{v}$ be a sufficiently regular test function. As $\Omega = \bigcup_{K\in\mathcal{T}_h} K$, by using the Green formulae, we have

$$\begin{aligned}\int_\Omega div(\sigma(\mathbf{u}))\cdot\mathbf{v}\,dx &= \sum_{K\in\mathcal{T}_h}\int_K div(\sigma(\mathbf{u}))\cdot\mathbf{v}\,dx \\ &= \sum_{K\in\mathcal{T}_h}\left(-\int_K \sigma(\mathbf{u})\cdot\nabla\mathbf{v}\,dx + \int_{\partial K}(\sigma(\mathbf{u})\mathbf{n})\cdot\mathbf{v}\,ds\right).\end{aligned} \tag{2.5}$$

Let $F = \partial K^+ \cap \partial K^-$, where K^+ and K^- denotes two neighboring elements, thus, we have

$$\sum_{K\in\mathcal{T}_h}\int_{\partial K}(\sigma(\mathbf{u})\mathbf{n})\cdot\mathbf{v}\,ds = \sum_{F\in\mathcal{F}_h}\int_F(\sigma(\mathbf{u}^+)\mathbf{n}^+)\cdot\mathbf{v}^+ + (\sigma(\mathbf{u}^-)\mathbf{n}^-)\cdot\mathbf{v}^-\,ds. \tag{2.6}$$

Using the relation $ab+cd = \frac{1}{2}(a+c)(b+d) + \frac{1}{2}(a-c)(b-d)$, we have

$$\begin{aligned}\int_F(\sigma(\mathbf{u}^+)\mathbf{n}^+)\cdot\mathbf{v}^+ + (\sigma(\mathbf{u}^-)\mathbf{n}^-)\cdot\mathbf{v}^-\,ds &= \int_F\frac{1}{2}(\sigma(\mathbf{u}^+)\mathbf{n}^+ + \sigma(\mathbf{u}^-)\mathbf{n}^-)\cdot(\mathbf{v}^+ + \mathbf{v}^-) \\ &\quad + \frac{1}{2}(\sigma(\mathbf{u}^+)\mathbf{n}^+ - \sigma(\mathbf{u}^-)\mathbf{n}^-)\cdot(\mathbf{v}^+ - \mathbf{v}^-)\,ds.\end{aligned} \tag{2.7}$$

For the pure elastic problem, the displacement $\mathbf{u}$ has a H^1-regularity with $\mathrm{div}(\sigma(\mathbf{u})) \in \mathbf{L}^2(\Omega)$. This implies that the following continuities through interior faces: $[\![\mathbf{u}]\!] = 0$ and $[\![\sigma(\mathbf{u})\mathbf{n}]\!] = 0$. Injecting these relations in (2.7) yields:

For all test functions, we have

$$\begin{aligned}\int_F(\sigma(\mathbf{u}^+)\mathbf{n}^+)\cdot\mathbf{v}^+ + (\sigma(\mathbf{u}^-)\mathbf{n}^-)\cdot\mathbf{v}^-\,ds &= \int_F\frac{1}{2}(\sigma(\mathbf{u}^+)\mathbf{n}^+ - \sigma(\mathbf{u}^-)\mathbf{n}^-)\cdot(\mathbf{v}^+ - \mathbf{v}^-)\,ds \\ &= \int_F\{\!\{\sigma(\mathbf{u})\mathbf{n}\}\!\}\cdot[\![\mathbf{v}]\!]\,ds.\end{aligned} \tag{2.8}$$

The equation (2.8) leads to the DG discretization of the elastic operator.
Let $\mathbf{u}_h, \mathbf{v}_h$ be the discrete solution and discrete test function respectively, then we have

$$a_h(\mathbf{u}_h,\mathbf{v}_h) := \sum_{K\in\mathcal{T}_h}\int_K\sigma(\mathbf{u}_h)\cdot\nabla\mathbf{v}_h\,dx - \sum_{F\in\mathcal{F}_h}\int_F\{\!\{\sigma(\mathbf{u}_h)\mathbf{n}\}\!\}\cdot[\![\mathbf{v}]\!]_h\,ds. \tag{2.9}$$

Unfortunately, it is well-known [21] that this approximation is not inf-sup stable because of the unsigned boundary term $\int_F\{\!\{\sigma(\mathbf{u}_h)\mathbf{n}\}\!\}\cdot[\![\mathbf{v}]\!]\,ds$. A sufficient condition to have the inf-sup

condition is the *coercivity* of the bilinear form $a_h(.,.)$. Now, we add terms which are sound with the problem. These terms are null for the continuous problem but they stabilize the discrete formulation. The first term added to obtain the *interior penalty discontinuous Galerkin* (IPDG) methods is called *penalty term*. This term (2.10) appears natural when looking at the coercivity proof (see [21] or next subsection)

$$\sum_{F\in\mathcal{F}_h}\int_F \alpha_F[\![\mathbf{u}_h]\!]\cdot[\![\mathbf{v}_h]\!]\,ds, \tag{2.10}$$

where $\alpha_F > 0$.

Another term is added to obtain the class of IPDG methods, which writes as

$$\varepsilon\sum_{F\in\mathcal{F}_h}\int_F [\![\mathbf{u}_h]\!]\cdot\{\!\{\sigma(\mathbf{v}_h)\mathbf{n}\}\!\}\,ds, \tag{2.11}$$

where $\varepsilon\in\{-1,0,1\}$. As we shall see this last term has a great impact on the properties of the method, namely the stability and the convergence rate.

Finally, the IPDG approximation for pure elastic problems is

$$\begin{aligned} a_h^e(\mathbf{u}_h,\mathbf{v}) = &\sum_{K\in\mathcal{T}_h}\int_K \sigma(\mathbf{u}_h)\cdot\nabla\mathbf{v}_h\,dx - \sum_{F\in\mathcal{F}_h}\int_F \{\!\{\sigma(\mathbf{u}_h)\mathbf{n}\}\!\}\cdot[\![\mathbf{v}_h]\!]\,ds \\ &+\varepsilon\sum_{F\in\mathcal{F}_h}\int_F [\![\mathbf{u}_h]\!]\cdot\{\!\{\sigma(\mathbf{v}_h)\mathbf{n}\}\!\}\,ds + \sum_{F\in\mathcal{F}_h}\int_F \alpha_F[\![\mathbf{u}_h]\!]\cdot[\![\mathbf{v}_h]\!]\,ds. \end{aligned} \tag{2.12}$$

2.2.2 IPDG for acoustic problems

Now, we consider a pure acoustic problem in displacement. In this case, the operator to discretize is $\mathrm{div}\sigma(\mathbf{u}) := \nabla(\lambda\mathrm{div}(\mathbf{u}))$ and the displacement has only a H-div regularity with $\nabla(\lambda\mathrm{div}(\mathbf{u}))\in\mathbf{L}^2$. This implies that the following continuities through each interior face: $[\![\mathbf{u}]\!]_N = 0$ and $[\![\mathrm{div}(\mathbf{u})]\!] = 0$. It immediately follows the following IPDG approximation:

$$\begin{aligned} a_h^a(\mathbf{u}_h,\mathbf{v}_h) = &\sum_{K\in\mathcal{T}_h}\int_K div(\mathbf{u}_h)\,div(\mathbf{v}_h)\,dx - \sum_{F\in\mathcal{F}_h}\int_F \{\!\{div(\mathbf{u}_h)\cdot\mathbf{n}\}\!\}\cdot[\![\mathbf{v}_h]\!]_N\,ds \\ &+\varepsilon\sum_{F\in\mathcal{F}_h}\int_F [\![\mathbf{u}_h]\!]_N\cdot\{\!\{div(\mathbf{v}_h)\cdot\mathbf{n}\}\!\}\,ds + \sum_{F\in\mathcal{F}_h}\int_F \alpha_F[\![\mathbf{u}_h]\!]_N\cdot[\![\mathbf{v}_h]\!]_N\,ds. \end{aligned} \tag{2.13}$$

where we denote by the subscript N and T the normal and tangential component of a vector relatively to a face.

2.2.3 IPDG for elasto-acoustic problems

Finally, we treat an elasto-acoustic interface (see Fig. 1). Due to the change of the functional nature between the two medium, we have the following transmission conditions:

$$\begin{cases} \mathbf{u}|_{\Omega_e}\cdot\mathbf{n} = \mathbf{u}|_{\Omega_a}\cdot\mathbf{n}, & \text{on } \Gamma, \\ \sigma(\mathbf{u}|_{\Omega_e})\mathbf{n} = -\lambda div(\mathbf{u}|_{\Omega_a})\mathbf{n}, & \text{on } \Gamma. \end{cases} \tag{2.14}$$

By decomposing $(\sigma(\mathbf{u}|_{\Omega_e})\mathbf{n})_N$ in the normal and the tangential component, we can rewrite these conditions as follow

$$\begin{cases} (\mathbf{u}|_{\Omega_e})_N = (\mathbf{u}|_{\Omega_a})_N, & \text{on } \Gamma, \\ (\sigma(\mathbf{u}|_{\Omega_e})\mathbf{n})_N = -\lambda div(\mathbf{u}|_{\omega_a}), & \text{on } \Gamma, \\ (\sigma(\mathbf{u}|_{\Omega_e})\mathbf{n})_T = 0, & \text{on } \Gamma, \end{cases} \tag{2.15}$$

where we denote by the subscript N and T the normal and tangential component of a vector relatively to a face.

Starting from (2.8), we decompose the normal and tangential component, we get:

$$\int_F \{\!\{\sigma(\mathbf{u})\mathbf{n}\}\!\} \cdot [\![\mathbf{v}]\!]\, ds = \int_F \{\!\{\sigma(\mathbf{u})\mathbf{n}\}\!\}_N \cdot [\![\mathbf{v}]\!]_N\, ds + \int_F \{\!\{\sigma(\mathbf{u})\mathbf{n}\}\!\}_T \cdot [\![\mathbf{v}]\!]_T\, ds. \tag{2.16}$$

Using that $\{\!\{\sigma(\mathbf{u})\mathbf{n}\}\!\}_T = 0$ on Γ (2.15), we get:

$$\int_F \{\!\{\sigma(\mathbf{u})\mathbf{n}\}\!\} \cdot [\![\mathbf{v}]\!]\, ds = \int_F \{\!\{\sigma(\mathbf{u})\mathbf{n}\}\!\}_N \cdot [\![\mathbf{v}]\!]_N\, ds. \tag{2.17}$$

Thus we get the bilinear form:

$$a_h^{ea}(\mathbf{u}_h, \mathbf{v}_h) = \sum_{K\in\mathcal{T}_h} \int_K \sigma(\mathbf{u}_h)\, \nabla \mathbf{v}_h\, dx - \sum_{F\in\mathcal{F}_h} \int_F \{\!\{\sigma(\mathbf{u}_h)\cdot\mathbf{n}\}\!\}_N \cdot [\![\mathbf{v}_h]\!]_N\, ds. \tag{2.18}$$

Now we can add the symmetric term and the penalty term:

$$\begin{aligned} a_h^{ea}(\mathbf{u}_h, \mathbf{v}_h) = &\sum_{K\in\mathcal{T}_h} \int_K \sigma(\mathbf{u}_h)\, \nabla \mathbf{v}_h\, dx - \sum_{F\in\mathcal{F}_h} \int_F \{\!\{\sigma(\mathbf{u}_h)\cdot\mathbf{n}\}\!\}_N \cdot [\![\mathbf{v}_h]\!]_N\, ds \\ &+ \varepsilon \sum_{F\in\mathcal{F}_h} \int_F [\![\mathbf{u}_h]\!]_N \cdot \{\!\{\sigma(\mathbf{v}_h)\cdot\mathbf{n}\}\!\}_N\, ds + \sum_{F\in\mathcal{F}_h} \int_F \alpha_F [\![\mathbf{u}_h]\!]_N \cdot [\![\mathbf{v}_h]\!]_N\, ds. \end{aligned} \tag{2.19}$$

Finally, we can express all these equations in one united formulation.This formulation simply does not control tangential fluxes unless the interface is purely elastic:

$$\begin{aligned} a_h(\mathbf{u}_h, \mathbf{v}_h) = &\sum_{K\in\mathcal{T}_h} \int_K \sigma(\mathbf{u}_h)\, \nabla \mathbf{v}_h\, dx \\ &- \sum_{F\in\mathcal{F}_h} \int_F \{\!\{\sigma(\mathbf{u}_h)\cdot\mathbf{n}\}\!\}_N \cdot [\![\mathbf{v}_h]\!]_N\, ds - \sum_{F\in\mathcal{F}_h} \int_F \Theta_F \{\!\{\sigma(\mathbf{u}_h)\cdot\mathbf{n}\}\!\}_T \cdot [\![\mathbf{v}_h]\!]_T\, ds \\ &+ \varepsilon \sum_{F\in\mathcal{F}_h} \int_F [\![\mathbf{u}_h]\!]_N \cdot \{\!\{\sigma(\mathbf{v}_h)\cdot\mathbf{n}\}\!\}_N\, ds + \varepsilon \sum_{F\in\mathcal{F}_h} \int_F \Theta_F [\![\mathbf{u}_h]\!]_T \cdot \{\!\{\sigma(\mathbf{v}_h)\cdot\mathbf{n}\}\!\}_T\, ds \\ &+ \sum_{F\in\mathcal{F}_h} \int_F \alpha_F [\![\mathbf{u}_h]\!]_N \cdot [\![\mathbf{v}_h]\!]_N\, ds. + \sum_{F\in\mathcal{F}_h} \int_F \Theta_F \alpha_F [\![\mathbf{u}_h]\!]_T \cdot [\![\mathbf{v}_h]\!]_T\, ds\,, \end{aligned} \tag{2.20}$$

where

$$\Theta_F = \begin{cases} 1 & \text{if Elastic-Elastic face,} \\ 0 & \text{otherwise.} \end{cases} \tag{2.21}$$

We define the local DG formulation a_h^K such that

$$a_h(\mathbf{u}, \mathbf{v}) = \sum_{K\in\mathcal{T}_h} a_h^K(\mathbf{u}, \mathbf{v}). \tag{2.22}$$

The bilinear function a_h^K are given by

$$\begin{aligned} a_h^K(\mathbf{u},\mathbf{v}) = &\int_K \sigma_h^K(\mathbf{u}) : \nabla \mathbf{v}\, dx \\ &- \sum_{F\in\mathcal{F}_h^K} \int_F \{\!\{\sigma_h(\mathbf{u})n\}\!\}_N \cdot \mathbf{v}_N\, d\gamma - \sum_{F\in\mathcal{F}_h^K} \int_F \Theta_F \{\!\{\sigma_h(\mathbf{u})n\}\!\}_T \cdot \mathbf{v}_T\, d\gamma \\ &+ \varepsilon \sum_{F\in\mathcal{F}_h^K} \int_F [\![\mathbf{u}]\!]_N \frac{1}{2}(\sigma_h^K(\mathbf{v})n)_N\, d\gamma + \varepsilon \sum_{F\in\mathcal{F}_h^K} \int_F \Theta_F [\![\mathbf{u}]\!]_T \frac{1}{2}(\sigma_h^K(\mathbf{v})n)_T\, d\gamma \\ &+ \sum_{F\in\mathcal{F}_h^K} \int_F \alpha_F [\![\mathbf{u}]\!]_N \cdot \mathbf{v}_N\, d\gamma + \sum_{F\in\mathcal{F}_h^K} \int_F \Theta_F \alpha_F [\![\mathbf{u}]\!]_T \cdot \mathbf{v}_T\, d\gamma. \end{aligned} \tag{2.23}$$

The general semi-discrete IPDG approximation of the model problem (2.3) is:

Find $\forall t \in [0,T], \mathbf{u}_h(.,t) \in V_h$ such that

$$\begin{cases} (\partial_{tt}\mathbf{u}_h, \mathbf{v}_h) + a_h(\mathbf{u}_h, \mathbf{v}_h) = (f, \mathbf{v}_h), \quad \forall \mathbf{v}_h \in V_h, \forall t \in [0,T], \\ \mathbf{u}_h|_{t=0} = \Pi_h u_0, \\ \partial_t \mathbf{u}_h|_{t=0} = \Pi_h v_0, \end{cases} \tag{2.24}$$

where Π_h denotes the L^2-projection onto V_h.

Let $K \in \mathcal{T}_h$, we denote by $\{\phi_i^K\}$ a basis of $V_h(K)$. Let $N_K = |\{\phi_i^K\}|$ be the number of degrees of freedom on element K and $N = \sum_{K\in\mathcal{T}_h} N_K$ is the total number of degrees of freedom.

The semi-discrete solution can be expanded in the global basis functions by

$$\forall t \in [0,T],\ \forall x \in \Omega, \quad \mathbf{u}_h(t,\mathbf{x}) = \sum_{K\in\mathcal{T}_h} \sum_{i=1}^{N_K} U_i^K(t)\phi_i^K(\mathbf{x}). \tag{2.25}$$

We note $\mathbf{U} := (U_i)_{1\le i\le N}$. The semi-discrete IPDG formulation (2.24) is equivalent to the second-order system of ordinary differential equations

$$\begin{cases} M\dfrac{d^2\mathbf{U}}{dt^2} + K\mathbf{U} = F, \\ \mathbf{U}(0) = \mathbf{U}_0, \\ \dfrac{d\mathbf{U}}{dt}(0) = \mathbf{V}_0, \end{cases} \tag{2.26}$$

where $M = (M_{ij})_{ij}$ is the $N \times N$ mass matrix, and $K = (K_{ij})_{ij}$ is the $N \times N$ stiffness matrix, and they are defined by

$$\forall i,j \in [\![1,N]\!] \quad M_{ij} = (\phi_j, \phi_i)_\Omega, \quad K_{ij} = a_h(\phi_j, \phi_i). \tag{2.27}$$

2.3 Space-time discretization

After discretizing the equation in space with a discontinuous Galerkin method, we finish the discretization of the problem using a finite difference method in time. This form is called the fully discretized IPDG formulation. We note by $\mathbf{U}^n$ the approximation of $\mathbf{U}(t_n)$ using the well-known finite difference second-order leap frog scheme for temporal derivatives. Hence, we get

$$M\frac{\mathbf{U}^{n+1} - 2\mathbf{U}^n + \mathbf{U}^{n-1}}{\Delta t^2} + K\mathbf{U}^n = F^n. \tag{2.28}$$

Full discrete local DG approximation: In the same way, we can rewrite the full discrete local DG approximation as

$$\forall K \in \mathcal{T}_h, \quad M^K \frac{\mathbf{u}_{n+1}^K - 2\mathbf{u}_n^K + \mathbf{u}_{n-1}^K}{\Delta t^2} + K^K \mathbf{u}_n^K + \sum_{F \in \mathcal{F}_K} F^{V_F(K)} \mathbf{u}_n^{V_F(K)} = l^K,$$

where

$$u_h^K(t_n, \mathbf{x}) := \sum_{i=1}^{N_K} u_{n,i}^K \varphi_i^K(\mathbf{x}), \quad \text{and} \quad \mathbf{u}_n^K := \left(u_{n,i}^K\right)_{1 \leq i \leq N^K}.$$

3 Optimized formulation

In this section, we want to introduce a new penalty and study its impact on the discontinuous Galerkin approximation of the stationary elasticity operator. Initially designed for scalar differential equations, these methods are usually directly transposed to vectorial differential equations. We found that this direct transposition comes with a weaken stability condition (the CFL condition). The previous analysis for elasto-acoustic media paves the way for an optimized penalty term suited for vectorial equations. The idea is to penalize differently normal and tangential parts of displacement in order to avoid an over penalization. In a homogeneous isotropic medium we can easily see that the normal part is associated with P-waves (that controls the divergence) and the tangential part with the S-waves (that controls the rotational). But the penalization used in the IPDG methods is usually only a function of the P-wave velocity v_P, which is always superior to the velocity of S-waves v_S. Therefore, this causes an "over-penalization" of the tangential part of the displacement. We propose to restore the dependence in v_S for the control of S-waves.

First, we state the following lemma, which will help us to reveal the polynomial order dependency in the coercivity constant, and thus the polynomial dependency of the penalty.

Lemma 1 (Inverse estimation [26])**.** *We have the following inverse estimation:*
Let $K \in \mathcal{T}_h$ and $\Gamma \subset \partial K$.

$$\forall \mathbf{u}_h \in V_h, \quad ||\mathbf{u}_h||_{L^2(\Gamma)} \leq C_{inv}(p) ||\mathbf{u}_h||_{L^2(K)},$$

where p is the polynomial order of the space $V_h(K)$.
For quadrangle elements and if $V_h(K) = Q_p(K)$ then $C_{inv}(p) = (p+1)\sqrt{\frac{|\partial K|}{|K|}}$.
For simplex elements and if $V_h(K) = P_p(K)$ then $C_{inv}(p) = \sqrt{\frac{(p+1)(p+d)}{d} \frac{|\partial K|}{|K|}}$ where d is the space dimension.

Our new discontinuous Galerkin approximation is:

$$\begin{aligned} a_h^{new,K}(\mathbf{u}, \mathbf{v}) = & \int_K \sigma_h^K(\mathbf{u}) : \nabla \mathbf{v} \, dx \\ & - \sum_{F \in \mathcal{F}_h^K} \int_F \{\!\{\sigma_h(\mathbf{u}) n\}\!\}_N \cdot \mathbf{v}_N \, d\gamma - \sum_{F \in \mathcal{F}_h^K} \int_F \Theta_F \{\!\{\sigma_h(\mathbf{u}) n\}\!\}_T \cdot \mathbf{v}_T \, d\gamma \\ & + \varepsilon \sum_{F \in \mathcal{F}_h^K} \int_F [\![\mathbf{u}]\!]_N \frac{1}{2} (\sigma_h^K(\mathbf{v}) n)_N \, d\gamma + \varepsilon \sum_{F \in \mathcal{F}_h^K} \int_F \Theta_F [\![\mathbf{u}]\!]_T \frac{1}{2} (\sigma_h^K(\mathbf{v}) n)_T \, d\gamma \\ & + \sum_{F \in \mathcal{F}_h^K} \int_F \alpha_{F,N} [\![\mathbf{u}]\!]_N \cdot \mathbf{v}_N \, d\gamma + \sum_{F \in \mathcal{F}_h^K} \int_F \Theta_F \alpha_{F,T} [\![\mathbf{u}]\!]_T \cdot \mathbf{v}_T \, d\gamma, \end{aligned} \tag{3.1}$$

where

$$\begin{aligned}
\alpha_{F,N} \,:\, \mathcal{F}_h^{\mathcal{I}} \cup \mathcal{F}_h^b &\rightarrow \mathbb{R} \\
F &\mapsto \alpha_{F,N} = \delta_N \frac{\{\!\{C_{inv}(p)^2(\lambda+2\mu)\}\!\}}{h_F}, \\
\alpha_{F,T} \,:\, \mathcal{F}_h^{\mathcal{I}} \cup \mathcal{F}_h^b &\rightarrow \mathbb{R} \\
F &\mapsto \alpha_{F,T} = \delta_T \frac{\{\!\{C_{inv}(p)^2\mu\}\!\}}{h_F},
\end{aligned} \tag{3.2}$$

with δ_N, $\delta_T \geq 0$ two real numbers, h_F the measure of the face F and $\mathcal{F}_h^b := \mathcal{F}_h^{\mathcal{B}} \cap \Gamma_D$.

We now verify that this formulation leads to a "good" approximation by studying the discrete inf-sup stability of this one. Actually, the stability constant gives an important information about the quality of the numerical solution. For that, we introduce the DG norm $||\cdot||_h$ by the following relation

$$\|\mathbf{v}_h\|_h^2 := \int_\Omega \sigma_h(\mathbf{v}_h) : \nabla_h \mathbf{v}_h \, d\mathbf{x} + \int_{\mathcal{F}_h^{\mathcal{I}} \cup \mathcal{F}_h^b} \alpha_{F,N} [\![\mathbf{v}_h]\!]_N [\![\mathbf{v}_h]\!]_N \, d\gamma + \int_{\mathcal{F}_h^{\mathcal{I}} \cup \mathcal{F}_h^b} \Theta_\Gamma \alpha_{F,T} [\![\mathbf{v}_h]\!]_T [\![\mathbf{v}_h]\!]_T \, d\gamma,$$

and we have the following theorem.

Theorem 1. *Given $C_{coer} \in]0,1[$. If $\varepsilon = 0$ or 1 and if we choose the penalty coefficients δ_N and δ_T as follows:*

$$\begin{aligned}
&\bullet \forall F \in \mathcal{F}_h^{\mathcal{I}},\ \delta_N,\, \delta_T \geq \delta_N^* = \delta_T^* := \frac{(1+\varepsilon)^2}{2(1-C_{coer})^2}, \\
&\bullet \forall F \in \mathcal{F}_h^b,\ \delta_N,\, \delta_T \geq \delta_N^* = \delta_T^* := \frac{(1+\varepsilon)^2}{(1-C_{coer})^2}. \\
&\bullet \forall F \in \mathcal{F}_h \cap \Gamma_N,\ \delta_N,\, \delta_T \geq \delta_N^* = \delta_T^* := 0.
\end{aligned} \tag{3.3}$$

where $N_K = \partial K \cap \mathcal{F}_h$. Thus, we have

$$\forall \mathbf{v}_h \in V_h, \quad a_h^{new,\varepsilon}(\mathbf{v}_h, \mathbf{v}_h) \geq C_{coer} \|\mathbf{v}_h\|_h^2. \tag{3.4}$$

Moreover, if $\varepsilon = -1$ then $\forall \delta_N,\, \delta_T \geq 0$,

$$a_h^{new,\varepsilon}(\mathbf{v}_h, \mathbf{v}_h) \quad = \quad \|\mathbf{v}_h\|_h^2,\ \forall \mathbf{v}_h \in V_h. \tag{3.5}$$

Proof. See Appendix A. The proof uses standard coercivity proof steps with the particularity to split the displacement into P-waves and S-waves components. □

Theorem 1 states that under the chosen penalty the bilinear form $a_h^{\text{new},\varepsilon}$ is coercive. There is a close link between the coercivity constant C_{coer} and the inf-sup constant β. Indeed, we have the relation:

$$\forall \mathbf{u}_h \in V_h, \quad \sup_{\mathbf{v}_h \in V_h} \frac{a_h^{\text{new},\varepsilon}(\mathbf{u}_h, \mathbf{v}_h)}{||\mathbf{v}_h||_h} \geq \frac{a_h^{\text{new},\varepsilon}(\mathbf{u}_h, \mathbf{u}_h)}{||\mathbf{u}_h||_h}.$$

Using the coercivity result we get

$$\forall \mathbf{u}_h \in V_h, \quad \sup_{\mathbf{v}_h \in V_h} \frac{a_h^{\text{new},\varepsilon}(\mathbf{u}_h, \mathbf{v}_h)}{||\mathbf{v}_h||_h} \geq C_{coer}||\mathbf{u}_h||_h.$$

Taking the infimum we get

$$\inf_{\mathbf{u}_h \in V_h} \sup_{\mathbf{v}_h \in V_h} \frac{a_h^{\text{new},\varepsilon}(\mathbf{u}_h, \mathbf{v}_h)}{||\mathbf{u}_h||_h||\mathbf{v}_h||_h} \geq C_{coer}.$$

Thus,

$$\beta \geq C_{coer}.$$

Moreover, if $\exists \mathbf{u}_h \in V_h$ such that $a_h^{\text{new},\varepsilon}(\mathbf{u}_h, \mathbf{u}_h) = C_{coer}||\mathbf{u}_h||_h^2$ then $\beta = C_{coer}$.

This means that the larger the coercivity constant is, the more the method is stable in the inf-sup sense and the closer the solution is to the optimal solution in V_h . However, the larger the coercivity constant is, the more stringent is the stability condition (CFL condition).

3.1 Dispersion - Dissipation

The plane wave analysis [9], although based on simplified problems, *i.e.*, infinite homogeneous medium, provides accurate information about the properties of a numerical method. This information is precise enough to be used in real simulations. It helps to apprehend two majors properties: dispersion and stability. The dispersion is a numerical phenomenon that creates a phase difference between the physical wave and the numerical wave, *i.e.*, the numerical velocity only approximates the physical velocity. The dispersion is used to determine the spatial discretization according to the desired precision, *i.e.*, the number of elements per wavelength that must be used to achieve the desired accuracy. Stability is given by a CFL condition which is a relation between the time step Δt and the space step h of the form $\frac{\Delta t}{h} \leq C$, where C is a constant that depends on physical and numerical parameters (dimension, polynomial approximation order, velocities).

The principle of a plane wave analysis is to seek the conditions, in the form of a discrete dispersion relation, for which a numerical plane wave is a solution of the scheme. Plane waves provide an accurate analysis because they constitute a basis of solution to the infinite homogeneous elastodynamic problem.

3.1.1 Dispersion relation formulation

In geoscience, having the correct propagation velocity is a major concern. Since direct propagations (the forward problem) are often used in the iterations of an inverse problem to know the structure of the ground, errors in propagation velocities result in bad ground imaging. Therefore, having a good control on the dispersion error is critical.

In order to get the dispersion relation, we begin with the local semi-discrete DG approximation in which we inject plane waves. By doing so, we get simple relations between all degrees of freedom. After some algebraic manipulations, we get a generalized eigenvalue problem that reveals which modes our numerical method propagates. Since a plane wave is monotonic our method should propagate only one mode, however the eigenvalue analysis reveals that more than one mode is propagated. We formulate the dispersion relation in an arbitrary dimension since the process is identical for any dimension.

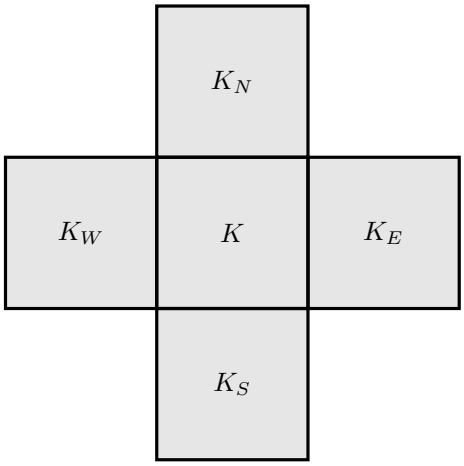

Figure 2: Neighboring elements of the element K.

The local DG approximation is

$$M\partial_{tt}\mathbf{u}^K + K\mathbf{u}^K + \sum_{f\in\mathcal{F}_K} F^f \mathbf{u}^{V_f(K)} = 0, \tag{3.6}$$

where

$$u_h^K(t,\mathbf{x}) = \sum_{i=1}^{N_K} u_i^K(t)\varphi_i^K(\mathbf{x}), \quad \text{with} \quad \mathbf{u}^K = \left(u_i^K\right)_{1\le i\le N^K},$$

and

$$M_{ij} = \rho_K(\varphi_j^K, \varphi_i^K)_K, \quad K_{ij} = a_h^K(\varphi_j^K, \varphi_i^K), \quad F_{ij}^f = a_h^K(\varphi_j^{V_f(K)}, \varphi_i^K).$$

Since the solution of this problem is a plane wave, we seek the numerical solution in the form of a discrete plane wave, then

$$u_j^K = A_j e^{-i(\mathbf{k}\cdot\mathbf{x}-\omega_h t)},$$

where $\mathbf{k}$ is the wavenumber, ω_h the pulsation and A_j the amplitude.
The plane wave assumption implies that

$$\mathbf{u}^{V_f(K)} = e^{i\mathbf{k}\cdot\mathbf{x}_f}\mathbf{u}^K, \tag{3.7}$$

where

$$\mathbf{x}_E = h\mathbf{e}_x, \quad \mathbf{x}_W = -h\mathbf{e}_x, \quad \mathbf{x}_N = h\mathbf{e}_y, \quad \mathbf{x}_S = -h\mathbf{e}_y, \quad \mathbf{x}_T = -h\mathbf{e}_z, \quad \mathbf{x}_B = h\mathbf{e}_z.$$

Injecting (3.7) in (3.6) yields the following generalized eigenvalue problem:

$$\omega_h^2 M\mathbf{u}^K + \left(K + \sum_{f\in\mathcal{F}_K} e^{i\mathbf{k}\cdot\mathbf{x}_f}F^f\right)\mathbf{u}^K = 0.$$

We choose a space step such that $h = \dfrac{\lambda}{N}$, where λ is the wavelength and $N \in \mathbb{N}^*$. Let $\mathbf{k} = k\mathbf{d}$, where $\mathbf{d}$ is a unit vector representing the direction of the wave. We introduce $\varkappa := \dfrac{1}{(p+1)N}$,

which corresponds to the inverse of points per wavelength, where p is the order of the polynomial space.

We get the relation

$$kh = 2\pi(p+1)\varkappa.$$

The eigenvalue problem becomes:

$$-h^2\omega_h^2\hat{M}\mathbf{u}^K + \left(\hat{K} + \sum_{f\in\mathcal{F}_K} e^{ikh(\mathbf{d}\cdot\mathbf{e}_f)}\hat{F}^f\right)\mathbf{u}^K = 0,$$

where $\hat{M} := \frac{1}{h^d}M$, $\hat{K} := \frac{1}{h^{2-d}}K$ and $\hat{F}^f := \frac{1}{h^{2-d}}F^f$.

We rewrite this problem as a function of $\varkappa$:

$$-(2\pi)^2(p+1)^2\varkappa^2\frac{\omega_h^2}{k^2}\hat{M}\mathbf{u}^K + \left(\hat{K} + \sum_{f\in\mathcal{F}_K} e^{i(2\pi)(p+1)\varkappa(\mathbf{d}\cdot\mathbf{e}_f)}\hat{F}^f\right)\mathbf{u}^K = 0.$$

We note that $\dfrac{\omega_h^2}{k^2}$ is an eigenvalue of the generalized eigenvalue problem:

$$\frac{\omega_h^2}{k^2}\hat{M}V = AV,$$

where

$$A = \frac{1}{(2\pi)^2(p+1)^2\varkappa^2}\left(\hat{K} + \sum_{f\in\mathcal{F}_K} e^{i(2\pi)(p+1)\varkappa(\mathbf{d}\cdot\mathbf{e}_f)}\hat{F}^f\right).$$

This eigenvalue problem posses $2(p+1)$ eigenvalues. However their is only four physical modes (two for P-waves and two for S-waves). Since the number of eigenvalues exceeds the number of physical modes we need to identify which modes correspond to the P-waves and S-waves.

$$v_h = \frac{\omega_h}{k}.$$

We define the dispersion error as follow:

$$e_p = \left|\frac{v_h}{v_p} - 1\right|, \quad e_s = \left|\frac{v_h}{v_s} - 1\right|,$$

where v_h is the numerical velocity of the mode given by the eigenvalue, and v_p and v_s are the expected velocities associated to P- and S-waves.

The dispersions e_p and e_s depend on the parameters p the polynomial order of the approximating space, $\varkappa$ the number of points per wavelength and $\mathbf{d}$ the direction of the waves.

3.1.2 Dispersion analysis

In this section, we apply a dispersion analysis to show the numerical properties of the dispersion. We used $v_p = 2600m.s^{-1}$, $v_s = 1300m.s^{-1}$ and $\rho = 2300kg.m^{-3}$ and a penalty parameter $\delta_N = \delta_T = 2$.

On Figure **??** and 3 we display the convergence of the maximal angular dispersion error ($\max_{\mathbf{u}} |e_p|$ and $\max_{\mathbf{u}} |e_s|$) according to the number of points per wavelength $\frac{1}{\varkappa}$ for different polynomial spaces. We observe that the convergence rates of the dispersion errors are $|e_p| = \mathcal{O}(h^{2k})$ and $|e_s| = \mathcal{O}(h^{2k})$, where k is the polynomial order of the space Q_k.

Remark 1. For NIPDG and IIPDG methods the dispersion errors convergence rates are $k+1$ for odd orders and k for even orders [23].

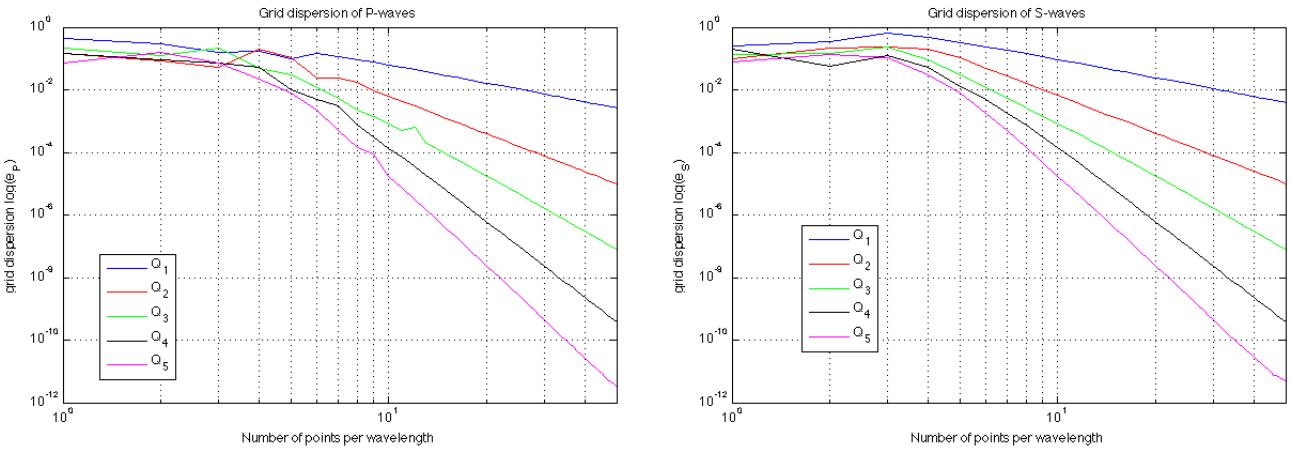

Figure 3: Dispersion error convergence for P-waves and S-waves for different polynomial basis according to the number of points per wavelength $\frac{1}{\varkappa}$.

On Figure 4 we compare the dispersion error for Q_3 elements with 10 points per wavelength with standard and optimized penalty. As we can see the results are almost the same for the P-waves dispersion and slightly better for the optimized penalty for the S-waves dispersion.

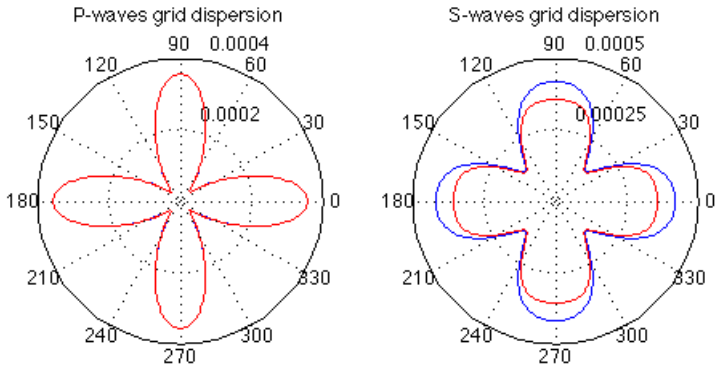

Figure 4: Comparison of the dispersion error with standard (in blue) and optimized penalty (in red) for Q_3 elements with 10 points per wavelength.

3.2 Stability condition: CFL

3.2.1 Stability condition formulation

We can use the previous analysis to derive the stability condition associated with our fully-discrete scheme. For that, we have to introduce the time discretization in the definition of the numerical plane wave. We thus have to inject the plane waves into the fully discretized DG approximation. By doing so, we get a relation between Δt and h.

The fully discrete local DG approximation is

$$M\frac{\mathbf{u}_{n+1}^K - 2\mathbf{u}_n^K + \mathbf{u}_{n-1}^K}{\Delta t^2} + K\mathbf{u}_n^K + \sum_{f\in\mathcal{F}_K} F^f \mathbf{u}_n^{K_f} = 0.$$

Since the solution of this problem is a plane wave, we seek the numerical solution in the form of a discrete plane wave, then

$$u_{n,j}^K = A_j e^{-i(\mathbf{k}\cdot\mathbf{x}_j^K - \omega_h n\Delta t)}.$$

Injecting this relation in the DG approximation yields

$$M\frac{e^{-i\omega_h\Delta t} - 2 + e^{i\omega_h\Delta t}}{\Delta t^2}\mathbf{u}_n^K + \left(K + \sum_{f\in\mathcal{F}_K} e^{i\mathbf{k}\cdot\mathbf{x}_f} F^f\right)\mathbf{u}_n^K = 0.$$

We reformulate the temporal term with some trigonometric relations

$$\frac{e^{-i\omega_h\Delta t} - 2 + e^{i\omega_h\Delta t}}{\Delta t^2} = \frac{2(\cos(\omega_h\Delta t) - 1)}{\Delta t^2} = -\frac{4\sin^2(\frac{\omega_h\Delta t}{2})}{\Delta t^2}.$$

Hence, we get the following generalized eigenvalue problem

$$-\frac{4h^2\sin^2(\frac{\omega_h\Delta t}{2})}{\Delta t^2}\hat{M}\mathbf{u}_n^K + \left(\hat{K} + \sum_{f\in\mathcal{F}_K} e^{i\mathbf{k}\cdot\mathbf{x}_f}\hat{F}^f\right)\mathbf{u}_n^K = 0, \tag{3.8}$$

where $\hat{M} = \frac{1}{h^d}M$, $\hat{K} = \frac{1}{h^{2-d}}K$ and $\hat{F}^f = \frac{1}{h^{2-d}}F^f$. We note that $\lambda = \dfrac{4h^2\sin^2(\frac{\omega_h\Delta t}{2})}{\Delta t^2}$ is an eigenvalue of our generalized eigenvalue problem. In order to have stability $\frac{4h^2\sin^2(\frac{\omega_h\Delta t}{2})}{\Delta t^2}$ has to be below all eigenvalues, yielding the following stability relation

$$\frac{\Delta t}{h} \leq \min_{1\leq j\leq N_K}\min_{0\leq\theta\leq 2\pi}\frac{2}{\sqrt{\Lambda_j(\theta)}}, \tag{3.9}$$

where $\{\Lambda_j\}_{1\leq j\leq N_K}$ are the eigenvalues of (3.8) according to the angle of incidence θ. We recall that N_K is the number of degrees of freedom per element.

3.2.2 CFL conditions

The CFL stability condition is a relation of the form

$$v_p\frac{\Delta t}{h} < C_{cfl}(k), \tag{3.10}$$

where $C_{cfl}(k)$ is the CFL constant depending on the polynomial order k of the polynomial spaces Q_k.

From the relation (3.9) we immediately get the value of the CFL constant:

$$C_{cfl}(k) = \frac{1}{v_p} \min_{1 \leq j \leq N_K} \min_{0 \leq \theta \leq 2\pi} \frac{2}{\sqrt{\Lambda_j(\theta)}}.$$

3.2.3 Comparing optimized and standard penalties

In this part, we compare the impact on the CFL condition of the optimized penalty introduced previously with the standard penalty. We note on Table 1 that the optimized penalty grants a gain for any polynomial degree of 33% in the CFL condition. These CFL constants have been calculated with the same velocities and penalty as the dispersion.

Space	Standard	Optimized	Gain
Q_1	0.150	0.199	33%
Q_2	0.0953	0.121	27%
Q_3	0.0420	0.0561	34%
Q_4	0.0319	0.0417	31%
Q_5	0.0194	0.0259	34%
Q_6	0.0158	0.0207	31%
Q_7	0.0111	0.0148	33%
Q_8	0.00941	0.0123	31%
Q_9	0.00724	0.00962	33%
Q_{10}	0.00622	0.00821	32%

Table 1: CFL conditions for different polynomial spaces Q_k for Gauss-Legendre basis functions with optimized and standard penalties.

4 Numerical results

In this part, we propose to show the relevance of our approach on two analytical comparisons and one illustrative example.

To achieve all our numerical experiments we bound the computational domain with second order PML [7] and we use a local time stepping method introduced by Diaz and Grote [6]. Spatial refinements are achieved through non-conforming nested Cartesian grids.

4.1 Two-layered medium

In this experiment we want to show the ability of the discontinuous Galerkin method without refinement to treat an heterogeneous case compared to the exact solution. In order to do so, we simply compare our solution to the analytical solution on a two-layered medium given by J. Diaz's code Gar6more [5].

We propose a simple test case made of a two layered medium. The top layer has the following characteristics: $\lambda = 1.9 \times 10^{10}$, $\mu = 5.5 \times 10^9$, $\rho = 3200\, kg.m^{-3}$, $v_p = 3061\, m.s^{-1}$ and $v_s = 1311\, m.s^{-1}$ and the bottom layer has the following characteristics: $\lambda = 7.7612 \times 10^{10}$, $\mu = 5.994 \times 10^9$, $\rho = 1850\, kg.m^{-3}$, $v_p = 4000\, m.s^{-1}$ and $v_s = 1800\, m.s^{-1}$. We positioned a pressure regularized Ricker source of central frequency $20Hz$ in the center of the medium, $50m$ above the

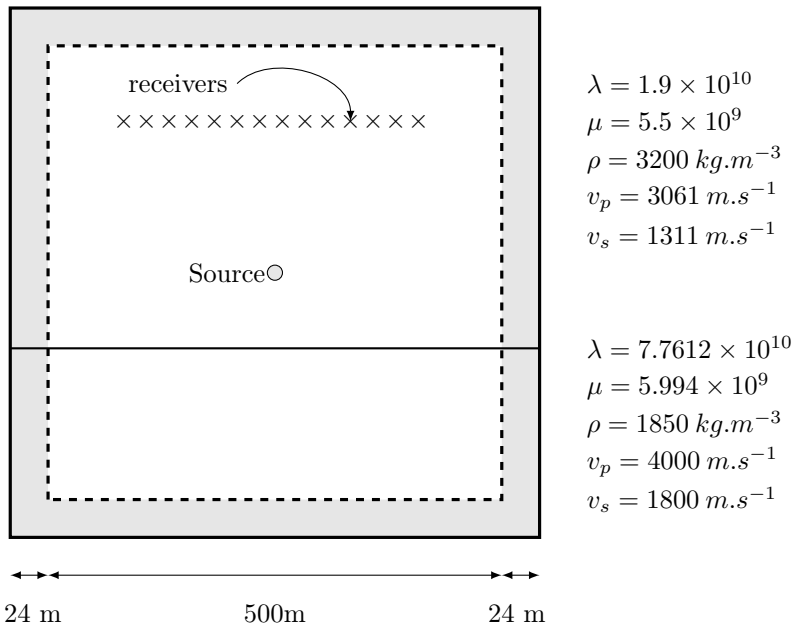

Figure 5: Two layered medium characteristics.

the two layers interface. We positioned a line of 100 receivers $150m$ above the interface from the abscissa $-200m$ up to $200m$.

The two different simulations displayed on Figure 6 and Figure 7, which are the analytical solution obtained from Gar6more and our solution made of Q_7 elements, these elements are of size $25m$. In order to compare these two simulations, we compare the line of seismograms for the displacement X and Y. We note that we obtained similar solutions with both methods, *i.e.*, arrival times and amplitudes are the same.

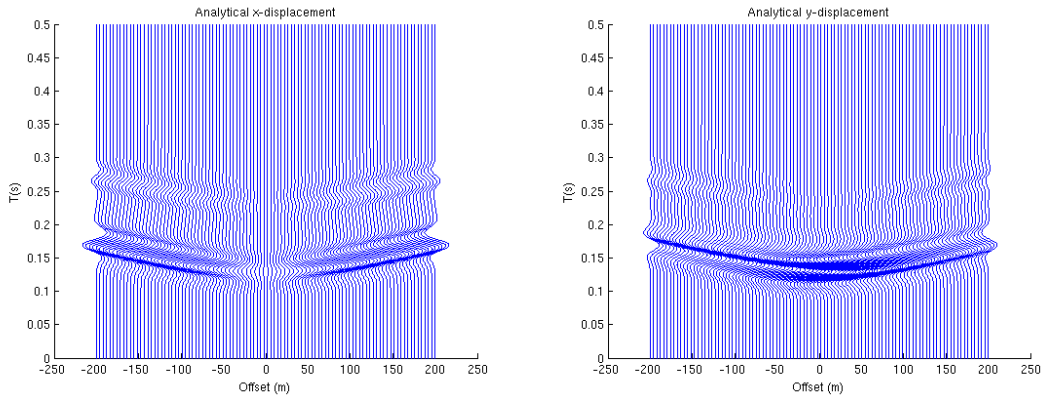

Figure 6: Analytical solution.

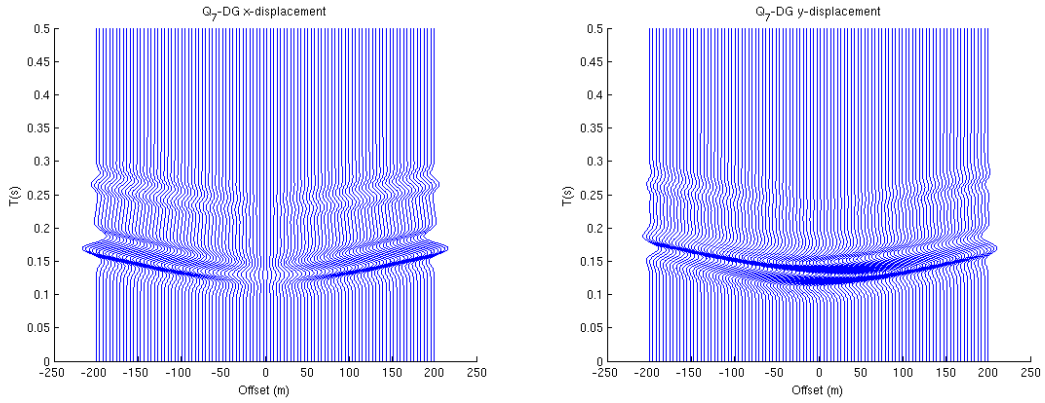

Figure 7: Discontinuous Galerkin solution.

4.2 Scattering by a hydro-fracture

The model geometry used to generate the seismograms is shown in Figure 8. The source, the receivers and hydro-fracture are located in an elastic medium ($v_p = 3500m.s^{-1}$, $v_s = 2023m.s^{-1}$ and $\rho = 2300kg.m^{-3}$). We used a pressure regularized Ricker source of central frequency $100Hz$ located at the origin. The seismograms are realized with 80 receivers disposed between $-200m$ and $200m$. The center line of the fracture lies between $(100m, -100m)$ and $(100m, 100m$, and is $1m$ wide. The hydro-fracture is modelled as a single crack represented by a relatively thin rectangle filled with water ($v_p = 1500m.s^{-1}$ and $\rho = 1020kg.m^{-3}$).

We used Q_5 elements, with a space step of $4m$. The refined area is spatially refined by a factor $p_s = 4$ with Q_5 elements, and temporally refined by a factor $p_t = 4$. We added $24m$ of PML around our domain.

We display on Figure 11 the seismograms we obtained, they can be compared with the ray-theoretical traveltimes on Figure 9 or they can also be compared to the seismograms displayed on Figure 10 obtained by indirect boundary element method [22]. Since the source is a pressure source, we expect only one P-wave incoming on the fracture. This P-wave is then transmitted inside the fracture into another P-wave, since there is no S-wave in acoustic media. Finally this P-wave is transmitted into a P-wave and an S-wave, this corresponds to the PPP- and PPS-waves front we have on Figure 9. There should also be some multiples due to the multiple reflections inside the hydro-fracture, however they must be of small amplitude since the angle of incidence is almost normal on the whole fracture. The tips of the fractures also generate some waves, called diffracted waves. Both P- and S-waves are diffracted from the incoming P-wave, this corresponds to PP_d- and PS_d-waves on Figure 9. We shall have the PPP-wave arriving first at the receivers, then the two PP_d-waves, then PPS-wave and finally the two PS_d-waves. Both Figure 9 and Figure 10 were extracted from [19]. We note that the seismograms (Figure 11) obtained with our method are similar to those obtained with the indirect boundary element method (Figure 10) and that we obtain all the reflected and diffracted waves predicted by ray-theory (Figure 9). These results validate our local elasto-acoustic approach since boundary element methods and ray-theory give robust reference solutions.

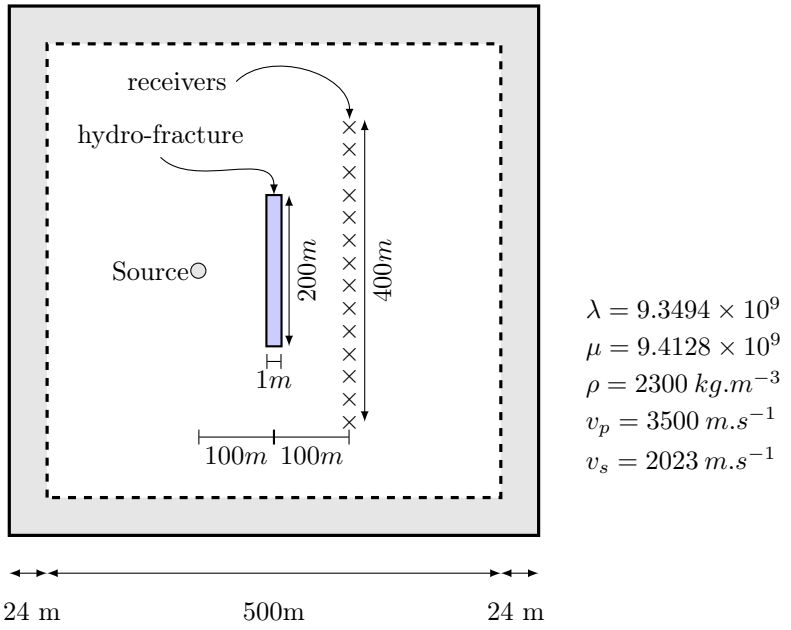

Figure 8: Medium with large hydro-fracture characteristics.

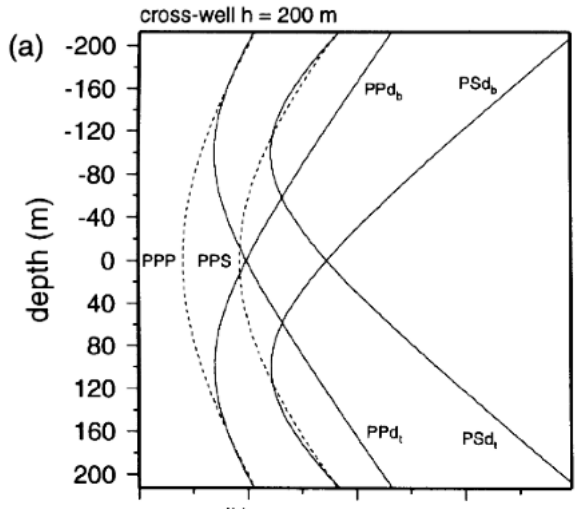

Figure 9: Ray-theoretical traveltimes extracted from [19].

4.3 Diffracting points

In this second illustrative experiment we want to show how tiny diffracting points filled with water can have a great impact on the simulation. However, the density of diffracting points (around 20%) is superior to what would be relevant for realistic simulations, this was intended in order to have visual snapshots.

We take the same homogeneous medium as in the previous test case with the characteristics:

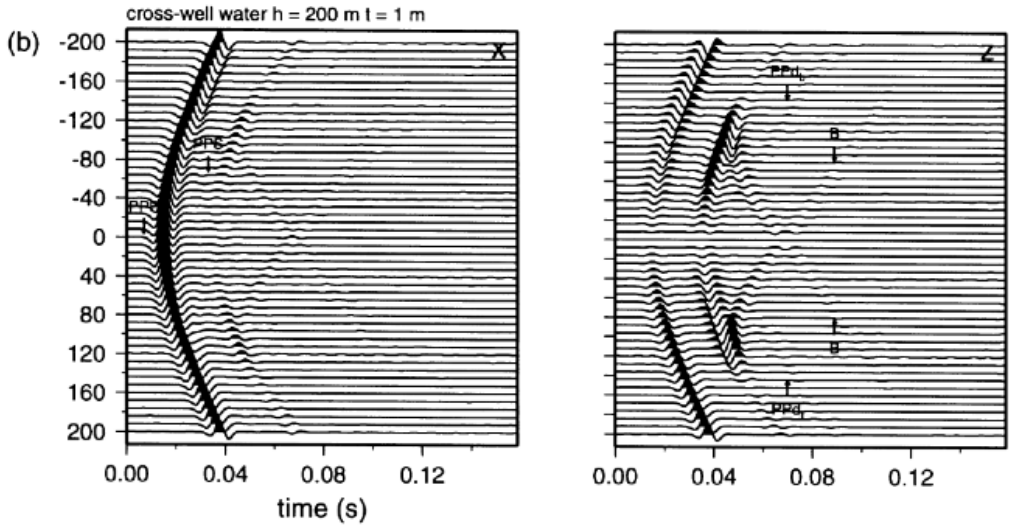

Figure 10: Reference seismograms extracted from [19].

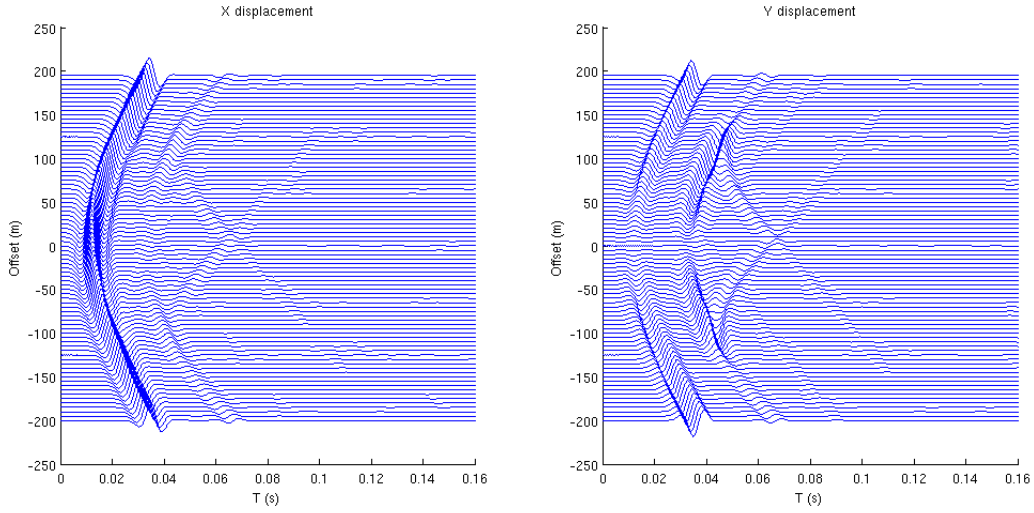

Figure 11: Seismograms.

$\lambda = 1.7612 \times 10^{10}$, $\mu = 5.994 \times 10^{9}$, $\rho = 1850\, kg.m^{-3}$, $v_p = 4000\, m.s^{-1}$ and $v_s = 1800\, m.s^{-1}$. We randomly inserted the diffracted points in a spatially refined area of dimension $40m \times 200m$, these points are squares of size $1m$ with water inside. We used a pressure regularized Ricker of central frequency $40Hz$ positioned in $(50m, 50m)$.

We used Q_5 elements, with a space step of $20m$. The refined area is spatially refined by a factor $p_s = 20$ with Q_1 elements, and temporally refined by a factor $p_t = 4$. We added $20m$ of PML around our domain.

We display on Figure 13 snapshots of X displacements. We note that the diffracting points produce an important diffraction that would not appear with elasticity only heterogeneities.

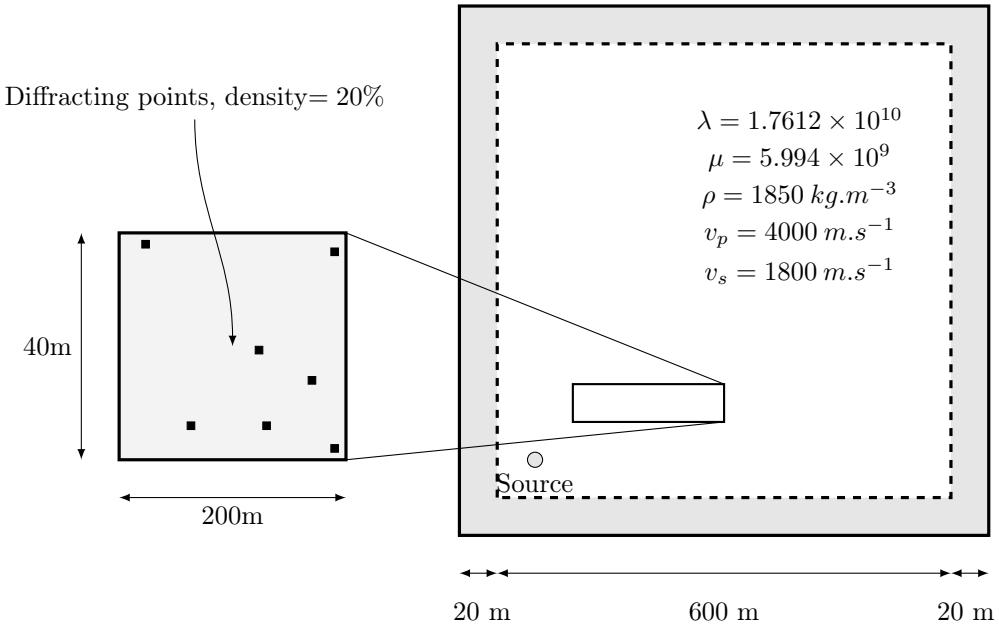

Figure 12: Diffracting points medium characteristics.

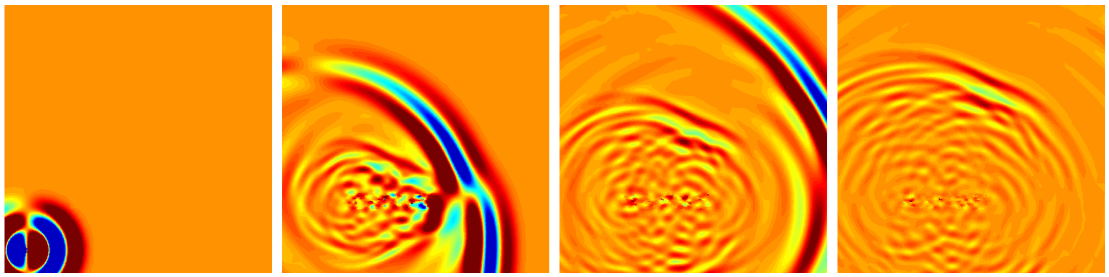

Figure 13: Snapshots at different times of X displacement for a medium with diffracting points.

5 Conclusion

The discontinuous Galerkin presented in this article is based on a displacement formulation both for acoustic and elastic domains to treat them in an unified framework. This unification is achieved through a simple change in the flux terms that guarantees the preservation of the right continuities. Consistency and stability of this scheme are proven and studied. Thus this scheme is adapted to 3D problems although we only showed 2D numerical experiments.

This elasto-acoustic formulation paved the way for an optimized formulation of interior penalty discontinuous Galerkin methods. Indeed, the optimized formulation leads to an improved numerical dispersion and 30% improved CFL condition for the elastodynamic equation. This decoupling of S-waves and P-waves penalty terms is applicable to other vectorial equations,

and similar improvements can be expected.

Although we did not discuss it in this paper, the new method is easily amenable to parallel implementation that is detailed in [7].

Acknowledgements

This work was partially supported by the company TOTAL. We thank Jean-Luc Boelle and Issam Tarrass from TOTAL for their enlightenment on geophysics.

A Proof of Theorem 1

In order to prove this result, it suffices to estimate the unsigned term

$$I_\Gamma := \int_\Gamma \{\!\{\sigma_h(\mathbf{v}_h)\mathbf{n}\}\!\}_N \cdot [\![\mathbf{v}_h]\!]_N \, d\gamma + \int_\Gamma \Theta_\Gamma \{\!\{\sigma_h(\mathbf{v}_h)\mathbf{n}\}\!\}_T \cdot [\![\mathbf{v}_h]\!]_T \, d\gamma, \tag{A.1}$$

for $\Gamma \in \mathcal{F}_h$.

- First case: $\Gamma = K \cap T \in \mathcal{F}_h^{\mathcal{I}}$.

  Using the Cauchy-Schwarz inequality in $\mathrm{L}^2(\Gamma)$:

$$\begin{aligned} I_\Gamma \leq & \frac{1}{2}\|(\sigma_h(\mathbf{v}_K)\mathbf{n})_N\|_{L^2(\Gamma)} \|[\![\mathbf{v}_h]\!]_N \|_{L^2(\Gamma)} + \frac{1}{2}\|(\sigma_h(\mathbf{v}_T)\mathbf{n})_N\|_{L^2(\Gamma)} \|[\![\mathbf{v}_h]\!]_N \|_{L^2(\Gamma)} \\ & + \frac{\Theta_\Gamma}{2}\|(\sigma_h(\mathbf{v}_K)\mathbf{n})_T\|_{L^2(\Gamma)} \|[\![\mathbf{v}_h]\!]_T \|_{L^2(\Gamma)} + \frac{\Theta_\Gamma}{2}\|(\sigma_h(\mathbf{v}_T)\mathbf{n})_T\|_{L^2(\Gamma)} \|[\![\mathbf{v}_h]\!]_T \|_{L^2(\Gamma)}. \end{aligned} \tag{A.2}$$

  We choose x to be normal to each face, and y tangential, we get

$$(\sigma(\mathbf{v})\mathbf{n}) \cdot \mathbf{n} = \lambda \mathrm{div}\mathbf{v} + 2\mu\partial_1\mathbf{v}_1, (\sigma(\mathbf{v})\mathbf{n}) \cdot \tau = \mu(\partial_2\mathbf{v}_1 + \partial_1\mathbf{v}_2). \tag{A.3}$$

  Introducing (A.3) in (A.2), we get:

$$\begin{aligned} I_\Gamma \leq & \frac{1}{2}\Big(\|\lambda_K \mathrm{div}\mathbf{v}_K + 2\mu_K\partial_1\mathbf{v}_{K,1}\|_{L^2(\Gamma)} + \|\lambda_T \mathrm{div}\mathbf{v}_T + 2\mu_T\partial_1\mathbf{v}_{T,1}\|_{L^2(\Gamma)}\Big)\|[\![\mathbf{v}_h]\!]_N \|_{L^2(\Gamma)} \\ & + \frac{\Theta_\Gamma}{2}\Big(\|\mu_K(\partial_2\mathbf{v}_{K,1} + \partial_1\mathbf{v}_{K,2})\|_{L^2(\Gamma)} + \|\mu_T(\partial_2\mathbf{v}_{T,1} + \partial_1\mathbf{v}_{T,2})\|_{L^2(\Gamma)}\Big)\|[\![\mathbf{v}_h]\!]_T \|_{L^2(\Gamma)}. \end{aligned} \tag{A.4}$$

  Using an inverse estimation, (A.4) becomes:

$$\begin{aligned} I_\Gamma \leq & \frac{1}{2}\Big(\frac{C_{inv}(p^K)}{h_\Gamma^{1/2}}\|\lambda_K \mathrm{div}\mathbf{v}_K + 2\mu_K\partial_1\mathbf{v}_{K,1}\|_{L^2(K)} \\ & + \frac{C_{inv}(p^T)}{h_\Gamma^{1/2}}\|\lambda_T \mathrm{div}\mathbf{v}_T + 2\mu_T\partial_1\mathbf{v}_{T,1}\|_{L^2(K)}\Big)\|[\![\mathbf{v}_h]\!]_N \|_{L^2(\Gamma)} \\ & + \frac{\Theta_\Gamma}{2}\Big(\frac{C_{inv}(p^K)}{h_\Gamma^{1/2}}\|\mu_K(\partial_2\mathbf{v}_{K,1} + \partial_1\mathbf{v}_{K,2})\|_{L^2(K)} \\ & + \frac{C_{inv}(p^T)}{h_\Gamma^{1/2}}\|\mu_T(\partial_2\mathbf{v}_{T,1} + \partial_1\mathbf{v}_{T,2})\|_{L^2(K)}\Big)\|[\![\mathbf{v}_h]\!]_T \|_{L^2(\Gamma)}. \end{aligned} \tag{A.5}$$

Applying a triangular inequality to (A.5) yields:

$$
\begin{aligned}
I_\Gamma \leq & \frac{1}{2}\Bigg(\frac{C_{inv}(p^K)}{h_\Gamma^{1/2}} \lambda_K^{1/2} \|\lambda_K^{1/2} \mathrm{div}\mathbf{v}_K\|_{L^2(K)} \\
& + \frac{C_{inv}(p^K)}{h_\Gamma^{1/2}} (2\mu_K)^{1/2} \|(2\mu_K)^{1/2} \partial_1 \mathbf{v}_{K,1}\|_{L^2(K)} \\
& + \frac{C_{inv}(p^T)}{h_\Gamma^{1/2}} \lambda_T^{1/2} \|\lambda_T^{1/2} \mathrm{div}\mathbf{v}_T\|_{L^2(T)} \\
& + \frac{C_{inv}(p^T)}{h_\Gamma^{1/2}} (2\mu_T)^{1/2} \|(2\mu_T)^{1/2} \partial_1 \mathbf{v}_{T,1}\|_{L^2(K)} \Bigg) \|[\![\mathbf{v}_h]\!]_N \|_{L^2(\Gamma)} \\
& + \frac{\Theta_\Gamma}{2}\Bigg(\frac{C_{inv}(p^K)}{h_\Gamma^{1/2}} \mu_K^{1/2} \|\mu_K^{1/2} (\partial_2 \mathbf{v}_{K,1} + \partial_1 \mathbf{v}_{K,2})\|_{L^2(K)} \\
& + \frac{C_{inv}(p^T)}{h_\Gamma^{1/2}} \mu_T^{1/2} \|(\mu_T)^{1/2} (\partial_2 \mathbf{v}_{T,1} + \partial_1 \mathbf{v}_{T,2})\|_{L^2(K)} \Bigg) \|[\![\mathbf{v}_h]\!]_T \|_{L^2(\Gamma)}.
\end{aligned}
\tag{A.6}
$$

If we sum on all faces of $\mathcal{F}_h^{\mathcal{I}}$ and use Cauchy-Schwarz inequality in $\mathbb{R}^N$ we get:

$$
\begin{aligned}
& \sum_{\substack{\Gamma \in \mathcal{F}_h^{\mathcal{I}} \\ \Gamma = K \cap T}} I_\Gamma \leq \\
& \frac{1}{2}\Bigg(\sum_{\substack{\Gamma \in \mathcal{F}_h^{\mathcal{I}} \\ \Gamma = K \cap T}} \|\lambda_K^{1/2} \mathrm{div}\mathbf{v}_K\|_{L^2(K)}^2 \Bigg)^{1/2} \Bigg(\sum_{\substack{\Gamma \in \mathcal{F}_h^{\mathcal{I}} \\ \Gamma = K \cap T}} \frac{C_{inv}(p^K)^2}{h_\Gamma} \lambda_K \|[\![\mathbf{v}_h]\!]_N \|_{L^2(\Gamma)}^2 \Bigg)^{1/2} \\
& + \frac{1}{2}\Bigg(\sum_{\substack{\Gamma \in \mathcal{F}_h^{\mathcal{I}} \\ \Gamma = K \cap T}} \|\lambda_T^{1/2} \mathrm{div}\mathbf{v}_T\|_{L^2(T)}^2 \Bigg)^{1/2} \Bigg(\sum_{\substack{\Gamma \in \mathcal{F}_h^{\mathcal{I}} \\ \Gamma = K \cap T}} \frac{C_{inv}(p^T)^2}{h_\Gamma} \lambda_T \|[\![\mathbf{v}_h]\!]_N \|_{L^2(\Gamma)}^2 \Bigg)^{1/2} \\
& + \frac{1}{2}\Bigg(\sum_{\substack{\Gamma \in \mathcal{F}_h^{\mathcal{I}} \\ \Gamma = K \cap T}} \|(2\mu_K)^{1/2} \partial_1 \mathbf{v}_{K,1}\|_{L^2(K)}^2 \Bigg)^{1/2} \Bigg(\sum_{\substack{\Gamma \in \mathcal{F}_h^{\mathcal{I}} \\ \Gamma = K \cap T}} \frac{C_{inv}(p^K)^2}{h_\Gamma} (2\mu_K) \|[\![\mathbf{v}_h]\!]_N \|_{L^2(\Gamma)}^2 \Bigg)^{1/2} \\
& + \frac{1}{2}\Bigg(\sum_{\substack{\Gamma \in \mathcal{F}_h^{\mathcal{I}} \\ \Gamma = K \cap T}} \|(2\mu_T)^{1/2} \partial_1 \mathbf{v}_{T,1}\|_{L^2(T)}^2 \Bigg)^{1/2} \Bigg(\sum_{\substack{\Gamma \in \mathcal{F}_h^{\mathcal{I}} \\ \Gamma = K \cap T}} \frac{C_{inv}(p^T)^2}{h_\Gamma} (2\mu_T) \|[\![\mathbf{v}_h]\!]_N \|_{L^2(\Gamma)}^2 \Bigg)^{1/2} \\
& + \frac{1}{2}\Bigg(\sum_{\substack{\Gamma \in \mathcal{F}_h^{\mathcal{I}} \\ \Gamma = K \cap T}} \|\mu_K^{1/2} (\partial_2 \mathbf{v}_{K,1} + \partial_1 \mathbf{v}_{K,2})\|_{L^2(K)}^2 \Bigg)^{1/2} \Bigg(\sum_{\substack{\Gamma \in \mathcal{F}_h^{\mathcal{I}} \\ \Gamma = K \cap T}} \Theta_\Gamma \frac{C_{inv}(p^K)^2}{h_\Gamma} \mu_K \|[\![\mathbf{v}_h]\!]_T \|_{L^2(\Gamma)}^2 \Bigg)^{1/2} \\
& + \frac{1}{2}\Bigg(\sum_{\substack{\Gamma \in \mathcal{F}_h^{\mathcal{I}} \\ \Gamma = K \cap T}} \|\mu_T^{1/2} (\partial_2 \mathbf{v}_{T,1} + \partial_1 \mathbf{v}_{T,2})\|_{L^2(T)}^2 \Bigg)^{1/2} \Bigg(\sum_{\substack{\Gamma \in \mathcal{F}_h^{\mathcal{I}} \\ \Gamma = K \cap T}} \Theta_\Gamma \frac{C_{inv}(p^T)^2}{h_\Gamma} \mu_T \|[\![\mathbf{v}_h]\!]_T \|_{L^2(\Gamma)}^2 \Bigg)^{1/2}.
\end{aligned}
$$

Finally, using Young's inequality $ab \leq \xi^2 a^2 + \frac{1}{4\xi^2} b^2$ we get:

$$\begin{aligned}
\sum_{\substack{\Gamma \in \mathcal{F}_h^{\mathcal{I}} \\ \Gamma = K \cap T}} I_\Gamma \leq & \frac{\xi^2}{2} \sum_{K \in \mathcal{T}_h} C(K) (\|\lambda_K^{1/2} \mathrm{div} \mathbf{v}_K\|^2_{L^2(K)} \\
& + \|\mu_K^{1/2} (\partial_2 \mathbf{v}_{K,1} + \partial_1 \mathbf{v}_{K,2})\|^2_{L^2(K)}) \\
& + \frac{\xi^2}{2} \sum_{K \in \mathcal{T}_h} C(K) \|(2\mu_K)^{1/2} \partial_1 \mathbf{v}_{K,1}\|^2_{L^2(K)} \\
& + \frac{\xi^2}{2} \sum_{K \in \mathcal{T}_h} C(K) \|(2\mu_K)^{1/2} \partial_2 \mathbf{v}_{K,2}\|^2_{L^2(K)} \\
& + \frac{1}{4\xi^2} \sum_{\substack{\Gamma \in \mathcal{F}_h^{\mathcal{I}} \\ \Gamma = K \cap T}} \frac{1}{h_\Gamma} \{\!\{ C_{inv}(p)^2 (\lambda + 2\mu) \}\!\} \| [\![\mathbf{v}_h]\!]_N \|^2_{L^2(\Gamma)} \\
& + \frac{1}{4\xi^2} \sum_{\substack{\Gamma \in \mathcal{F}_h^{\mathcal{I}} \\ \Gamma = K \cap T}} \frac{\Theta_\Gamma}{h_\Gamma} \{\!\{ C_{inv}(p)^2 \mu \}\!\} \| [\![\mathbf{v}_h]\!]_T \|^2_{L^2(\Gamma)},
\end{aligned} \tag{A.8}$$

where $C(K) \leq N_K$ is the cardinal number of $\partial K \cap \mathcal{F}_h^{\mathcal{I}}$ and $N_K = \partial K \cap \mathcal{F}_h$.

- Second case: $\Gamma \in \mathcal{F}_h^b$ such that $\Gamma \subset \partial K$. Proceeding as in the first case, we immediately get:

$$\begin{aligned}
\sum_{\substack{\Gamma \in \mathcal{F}_h^{b} \\ \Gamma \subset \partial K}} I_\Gamma \leq & \xi_b^2 \sum_{K \in \mathcal{T}_h} C_b(K) (\|\lambda_K^{1/2} \mathrm{div} \mathbf{v}_K\|^2_{L^2(K)} \\
& + \|\mu_K^{1/2} (\partial_2 \mathbf{v}_{K,1} + \partial_1 \mathbf{v}_{K,2})\|^2_{L^2(K)}) \\
& + \xi_b^2 \sum_{K \in \mathcal{T}_h} C_b(K) \|(2\mu_K)^{1/2} \partial_1 \mathbf{v}_{K,1}\|^2_{L^2(K)} \\
& + \xi_b^2 \sum_{K \in \mathcal{T}_h} C_b(K) \|(2\mu_K)^{1/2} \partial_2 \mathbf{v}_{K,2}\|^2_{L^2(K)} \\
& + \frac{1}{4\xi_b^2} \sum_{\substack{\Gamma \in \mathcal{F}_h^{b} \\ \Gamma \subset \partial K}} \frac{1}{h_\Gamma} \{\!\{ C_{inv}(p)^2 (\lambda + 2\mu) \}\!\} \| [\![\mathbf{v}_h]\!]_N \|^2_{L^2(\Gamma)} \\
& + \frac{1}{4\xi_b^2} \sum_{\substack{\Gamma \in \mathcal{F}_h^{b} \\ \Gamma \subset \partial K}} \frac{\Theta_\Gamma}{h_\Gamma} \{\!\{ C_{inv}(p)^2 \mu \}\!\} \| [\![\mathbf{v}_h]\!]_T \|^2_{L^2(\Gamma)},
\end{aligned} \tag{A.9}$$

where $C_b(K) \leq N_K$ is the cardinal number of $\partial K \cap \mathcal{F}_h^b$.

- Using the definition of the isotropic stress tensor, we get:

$$\int_\Omega \sigma_h(\mathbf{v}_h) : \nabla_h \mathbf{v}_h \, d\mathbf{x} = \sum_{K\in\mathcal{T}_h} (\|\lambda_K^{1/2}\mathrm{div}\mathbf{v}_K\|^2_{L^2(K)} + \|(2\mu_K)^{1/2}\partial_1\mathbf{v}_{K,1}\|^2_{L^2(K)} + \|(2\mu_K)^{1/2}\partial_2\mathbf{v}_{K,2}\|^2_{L^2(K)} + \|\mu_K^{1/2}(\partial_2\mathbf{v}_{K,1}+\partial_1\mathbf{v}_{K,2})\|^2_{L^2(K)}). \tag{A.10}$$

If we look now the coercivity of the form $a_h^{\mathrm{new},\varepsilon}$:

Using (A.8), (A.9) et (A.10), we have

$$\begin{aligned}
a_h^{\mathrm{new},\varepsilon}(\mathbf{v}_h,\mathbf{v}_h) = &\int_\Omega \sigma_h(\mathbf{v}_h) : \nabla_h \mathbf{v}_h \, d\mathbf{x} \\
&- (1+\varepsilon)\int_{\mathcal{F}_h} \{\!\{\sigma_h(\mathbf{v}_h)\mathbf{n}\}\!\}_N \cdot [\![\mathbf{v}_h]\!]_N \, d\gamma \\
&- (1+\varepsilon)\int_{\mathcal{F}_h} \Theta_\Gamma \{\!\{\sigma_h(\mathbf{v}_h)\mathbf{n}\}\!\}_T \cdot [\![\mathbf{v}_h]\!]_T \, d\gamma \\
&+ \sum_{\Gamma\in\mathcal{F}_h^{\mathcal{I}}\cup\mathcal{F}_h} \delta_N \frac{\{\!\{C_{inv}(p)^2(\lambda+2\mu)\}\!\}}{h_\Gamma} \|[\![\mathbf{v}_h]\!]_N\|^2_{L^2(\Gamma)} \\
&+ \sum_{\Gamma\in\mathcal{F}_h^{\mathcal{I}}\cup\mathcal{F}_h} \delta_T \frac{\Theta_\Gamma\{\!\{C_{inv}(p)^2\mu\}\!\}}{h_\Gamma} \|[\![\mathbf{v}_h]\!]_T\|^2_{L^2(\Gamma)} \\
\geq &\sum_{K\in\mathcal{T}_h} \Big((1-(1+\varepsilon)(\xi_b^2 C_b(K) + \frac{\xi^2}{2}C(K)))\|\lambda_K^{1/2}\mathrm{div}\mathbf{v}_K\|^2_{L^2(K)} \\
&+ (1-(1+\varepsilon)(\xi_b^2 C_b(K) + \frac{\xi^2}{2}C(K)))\|(2\mu_K)^{1/2}\partial_1\mathbf{v}_{K,1}\|^2_{L^2(K)} \\
&+ (1-(1+\varepsilon)(\xi_b^2 C_b(K) + \frac{\xi^2}{2}C(K)))\|(2\mu_K)^{1/2}\partial_2\mathbf{v}_{K,2}\|^2_{L^2(K)} \\
&+ (1-(1+\varepsilon)(\xi_b^2 C_b(K) + \frac{\xi^2}{2}C(K)))\|\mu_K^{1/2}(\partial_2\mathbf{v}_{K,1}+\partial_1\mathbf{v}_{K,2})\|^2_{L^2(K)} \Big) \\
&+ \sum_{\Gamma\in\mathcal{F}_h^{\mathcal{I}}} (1-\frac{(1+\varepsilon)}{4\xi^2\delta_N})\delta_N \frac{\{\!\{C_{inv}(p)^2(\lambda+2\mu)\}\!\}}{h_\Gamma} \|[\![\mathbf{v}_h]\!]_N\|^2_{L^2(\Gamma)} \\
&+ \sum_{\Gamma\in\mathcal{F}_h^{\mathcal{I}}} (1-\frac{(1+\varepsilon)}{4\xi^2\delta_T})\delta_T \frac{\Theta_\Gamma\{\!\{C_{inv}(p)^2\mu\}\!\}}{h_\Gamma} \|[\![\mathbf{v}_h]\!]_T\|^2_{L^2(\Gamma)} \\
&+ \sum_{\Gamma\in\mathcal{F}_h^{\mathcal{I}}} (1-\frac{(1+\varepsilon)}{4\xi^2\delta_N})\delta_N \frac{\{\!\{C_{inv}(p)^2(\lambda+2\mu)\}\!\}}{h_\Gamma} \|[\![\mathbf{v}_h]\!]_N\|^2_{L^2(\Gamma)}
\end{aligned}$$

Since $C_b(K) + C(K) = N_K$, choosing $\xi_b^2 = \xi^2/2$, we get

$$(1 - (1+\varepsilon)(\xi_b^2 C_b(K) + \frac{\xi^2}{2} C(K))) = 1 - \frac{N_K(1+\varepsilon)\xi^2}{2}.$$

We want a relation such that $\forall u \in V_h, a(u,u) \geq C_{coer}||u||_h$.

To get a coercivity constant $C_{coer} \in]0,1[$ when $\varepsilon \in \{0,1\}$, we need to have

$$1 - \frac{N_K(1+\varepsilon)\xi^2}{2} \geq C_{coer}$$

and

$$1 - \frac{(1+\varepsilon)}{2\xi^2\delta_N} \geq C_{coer}$$

and

$$1 - \frac{(1+\varepsilon)}{2\xi^2\delta_T} \geq C_{coer}$$

Thus, we have to choose

$$\forall \Gamma \in \mathcal{F}_h,\ \delta_N,\ \delta_T \geq \delta_N^* = \delta_T^* := \frac{N_K(1+\varepsilon)^2}{4(1-C_{coer})^2}. \tag{A.12}$$

References

[1] Emmanuel Bossy. *Evaluation ultrasonore de l'os cortical par transmission axiale : modélisation et expérimentation in vitro et in vivo.* Theses, Université Pierre et Marie Curie - Paris VI, July 2003. Jury: Anne-Sophie Bonnet-Ben Dhia, Pierre-Yves Hennion, Jean-Denis Laredo, Pascal Laugier, Frédéric Patat, Patrick Rasolofosaon, Maryline Talmant.

[2] S.C. Brenner and L. Ridgway Scott. *The Finite Element Method for Solid and Structural Mechanics.* McGraw Hill, New York, 2008.

[3] Emmanuel Chaljub, Yann Capdeville, and Jean-Pierre Vilotte. Solving elastodynamics in a fluid-solid heterogeneous sphere: A parallel spectral element approximation on non-conforming grids. *J. Comput. Phys.*, 187(2):457–491, May 2003.

[4] G Derveaux. *Modélisation numérique de la guitare acoustique.* PhD thesis, Ecole Polytechnique, 2002.

[5] J. Diaz and A. Ezziani. Gar6more 2d, 2008.

[6] Julien Diaz and J. Grote, Marcus. Energy conserving explicit local time stepping for second-order wave equations. In *The 8th International Conference on Mathematical and Numerical Aspects of Waves Propagation (WAVES 2007)*, Reading, Royaume-Uni, 2007.

[7] Yohann Dudouit. *Spatio-temporal refinement using a discontinuous Galerkin approach for elastodynamic in a high performance computing framework.* PhD thesis, University of Bordeaux, 2014.

[8] Bengt Fornberg. The pseudospectral method; accurate representation of interfaces in elastic wave calculations. *Geophysics*, 53(5):625–637, 1988.

[9] Cohen Gary. *Higher-Order Numerical Methods for Transient Wave Equations*. Springer, 2002.

[10] J.S. Hesthaven and T. Warburton. *Nodal discontinuous Galerkin methods: algorithms, analysis, and applications*. Springer, 2008.

[11] Randall Wade Hoberecht, Randall W. Hoberecht, Randall J. Leveque, J. Nathan Kutz, and Randall Wade Hoberecht. A finite volume approach to modeling injury mechanisms of blast-induced traumatic brain injury, 2009.

[12] Zhang Jianfeng and Liu Tielin. P-SV-wave propagation in heterogeneous media: grid method. *Geophysical Journal International*, 136(2):431–438, 1999.

[13] Zhang Jianfeng and Liu Tielin. Elastic wave modelling in 3D heterogeneous media: 3D grid method. *Geophysical Journal International*, 150(3):780–799, 2002.

[14] D. Komatitsch, C. Barnes, and J. Tromp. Wave propagation near a fluid-solid interface: a spectral element approach. 65(2):623–631, 2000.

[15] Dan D. Kosloff and Edip Baysal. Forward modeling by a fourier method. *Geophysics*, 47(10):1402–1412, 1982.

[16] R.J. Leveque. *Finite volume methods for hyperbolic problems*. Cambridge University Press, New-York, USA, 2002.

[17] Bruno Lombard and Joël Piraux. Numerical treatment of two-dimensional interfaces for acoustic and elastic waves. *J. Comput. Phys.*, 195(1):90–116, March 2004.

[18] Peter Moczo, Johan O.A. Robertsson, and Leo Eisner. The finite-difference time-domain method for modeling of seismic wave propagation. In Valerie Maupin Ru-Shan Wu and Renata Dmowska, editors, *Advances in Wave Propagation in Heterogenous Earth*, volume 48 of *Advances in Geophysics*, pages 421 – 516. Elsevier, 2007.

[19] Tim Pointer, Enru Liu, and John A. Hudson. Numerical modelling of seismic waves scattered by hydrofractures: application of the indirect boundary element method. *Geophysical Journal International*, 135(1):289–303, 1998.

[20] Enrico Priolo, José M. Carcione, and Géza Seriani. Numerical simulation of interface waves by high-order spectral modeling techniques. *The Journal of the Acoustical Society of America*, 95(2):681–693, 1994.

[21] Beatrice Riviere. *Discontinuous Galerkin Methods For Solving Elliptic And Parabolic Equations: Theory and Implementation*. Society for Industrial and Applied Mathematics, Philadelphia, PA, USA, 2008.

[22] A. Rodríguez-Castellanos, E. Flores, F.J. Sánchez-Sesma, C. Ortiz-Alemán, M. Nava-Flores, and R. Martin. Indirect boundary element method applied to fluid-solid interfaces. *Soil Dynamics and Earthquake Engineering*, 31(3):470 – 477, 2011.

[23] Shuyu Sun and Mary F. Wheeler. Discontinuous Galerkin methods for coupled flow and reactive transport problems. *Applied Numerical Mathematics*, 52(2-3):273 – 298, 2005. {ADAPT} '03: Conference on Adaptive Methods for Partial Differential Equations and Large-Scale Computation.

[24] Jean Virieux. P-SV wave propagation in heterogeneous media; velocity-stress finite-difference method. *Geophysics*, 51(4):889–901, 1986.

[25] P. Voinovich, A. Merlen, E. Timofeev, and K. Takayama. A godunov-type finite-volume scheme for unified solid-liquid elastodynamics on arbitrary two-dimensional grids. *Shock Waves*, 13(3):221–230, 2003.

[26] T Warburton and J Hesthaven. On the constants in hp-finite element trace inverse inequalities. *Computer Methods in Applied Mechanics and Engineering*, 192:pp. 2765–2773, 2003.

[27] Lucas C. Wilcox, Georg Stadler, Carsten Burstedde, and Omar Ghattas. A high-order discontinuous galerkin method for wave propagation through coupled elastic-acoustic media. *Journal of Computational Physics*, 229(24):9373 – 9396, 2010.

[28] Kane Yee. Numerical solution of initial boundary value problems involving Maxwell's equations in isotropic media. *Antennas and Propagation, IEEE Transactions on*, 14(3):302–307, May 1966.

[29] O.C. Zienkewicz. *Finite elements and approximation.* J. Wiley and Sons, New York, 1983.

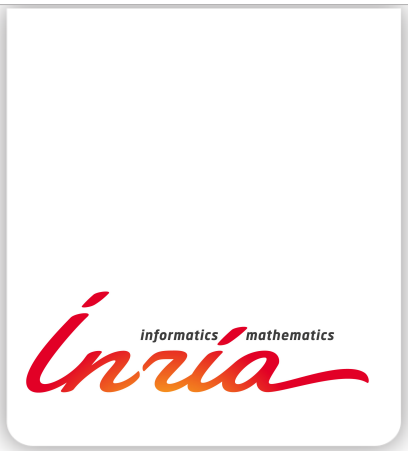

RESEARCH CENTRE
BORDEAUX – SUD-OUEST

200 avenue de la Vielle Tour
33405 Talence Cedex

Publisher
Inria
Domaine de Voluceau - Rocquencourt
BP 105 - 78153 Le Chesnay Cedex
inria.fr

ISSN 0249-6399